

Supplemental material for

Injured epithelial cell states impact kidney allograft survival after T-cell-mediated rejection

Anna Maria Pfefferkorn^{1,*}, Lorenz Jahn^{2,*}, Patrick T. Gauthier^{3,4,*}, Vera Anna Kulow⁵, Johannes Roeles^{2,6}, Niklas Müller-Böttcher^{7,8}, Louisa M. S. Gerhardt⁹, Janna Leiz², Sadia Sarfraz¹, Izabela Plumbom^{10,11}, Robert Greite², Svjetlana Lovric², Jaba Gamrekashvili², Florian Limbourg², Jessica Schmitz¹², Jan Hinrich Bräsen¹², Irina Scheffner², Igor M. Sauer¹, Felix Aigner^{1,13}, Janine Altmüller^{10,11}, Thomas Conrad^{10,11}, Wilfried Gwinner², Naveed Ishaque⁷, Michael Fähling⁵, Kai M. Schmidt-Ott², Philip F. Halloran^{3,4,#}, Muhammad Imtiaz Ashraf^{1,#}, Christian Hinze^{2,#}

1 Department of Surgery, Experimental Surgery, Charité – Universitätsmedizin Berlin, corporate member of Freie Universität Berlin, Humboldt-Universität zu Berlin and Berlin Institute of Health, Berlin, Germany

2 Department of Nephrology and Hypertension, Hannover Medical School, Hannover, Germany

3 Alberta Transplant Applied Genomics Centre, Edmonton, Alberta, Canada

4 Department of Medicine, Division of Nephrology and Transplant Immunology, University of Alberta, Edmonton, Alberta, Canada.

5 Institute of Translational Physiology, Charité – Universitätsmedizin Berlin, corporate member of Freie Universität Berlin and Humboldt-Universität zu Berlin, Berlin, Germany

6 PRACTIS Clinician Scientist Program, Dean's Office for Academic Career Development, Hannover Medical School, Germany

7 Berlin Institute of Health at Charité – Universitätsmedizin Berlin, Center of Digital Health, Berlin, Germany

8 Freie Universität Berlin, Department of Mathematics and Computer Science, Berlin, Germany

9 Department of Medicine V, University Medical Centre Mannheim, University of Heidelberg, Mannheim, Germany

10 Genomics Technology Platform, Max Delbrück Center for Molecular Medicine, Berlin, Germany

11 Core Unit Genomics, Berlin Institute of Health at Charité, Berlin, Germany

12 Nephropathology Unit, Institute of Pathology, Hannover Medical School, Hannover, Germany

13 Department of Surgery, Krankenhaus der Barmherzigen Brüder, Graz, Austria

* These authors contributed equally

These authors jointly supervised this work

Corresponding authors:

Prof. Dr. Philip F. Halloran, Email: phallora@ualberta.ca

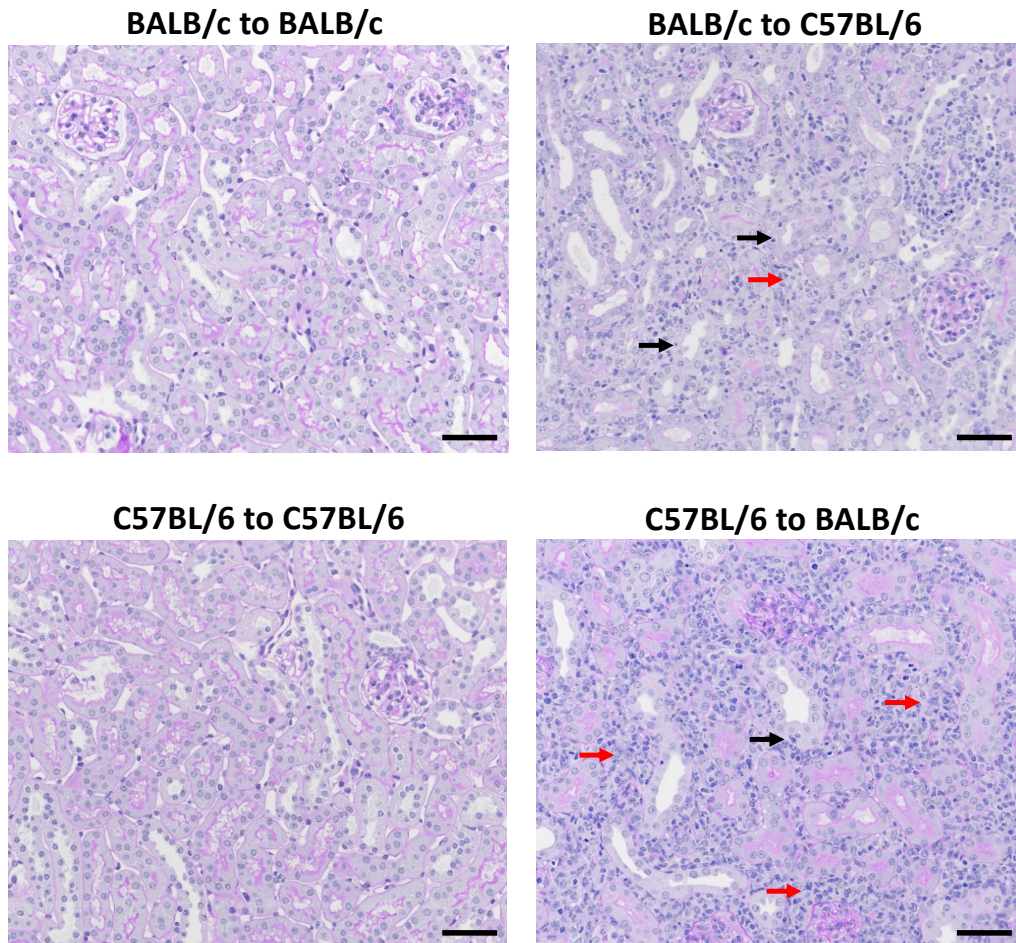
Dr. Muhammad Imtiaz Ashraf, Email: muhammad-imtiaz.ashraf@charite.de

Prof. Dr. Christian Hinze, Email: hinze.christian@mh-hannover.de

A

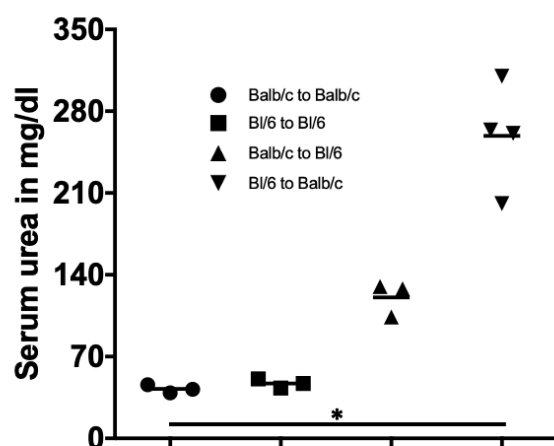
Group	Tx combination	Mouse IDs	Sample name in manuscript (if applicable)	Used for clinical analyses (creatinine etc.)	snRNA-seq	ST	Banff scoring		
							i	t	v
SYN	C57BL/6 - C57BL/6	M1	C57BL/6 to C57BL/6 1	x	x	x	0	0	0
SYN		M2		x			0	0	0
SYN		M3		x			0	0	0
SYN	Balb/c - Balb/c	M1	BALB/c to BALB/c 1	x	x	x	0	0	0
SYN		M2	BALB/c to BALB/c 2	x	x		0	0	0
SYN		M3		x			0	0	0
ALLO	Balb/c - C57BL/6	M1	BALB/c to C57BL/6 1	x	x	x	2	1	1
ALLO		M2		x			2	2	1
ALLO		M3	BALB/c to C57BL/6 3	x	x	x	3	1	1
ALLO	C57BL/6 - Balb/c	M1	C57BL/6 to BALB/c 1	x	x	x	3	1	1
ALLO		M2	C57BL/6 to BALB/c 2	x	x	x	3	3	1
ALLO		M3	C57BL/6 to BALB/c 3	x	x	x	3	2	1
ALLO		M4		x			3	2	1

B



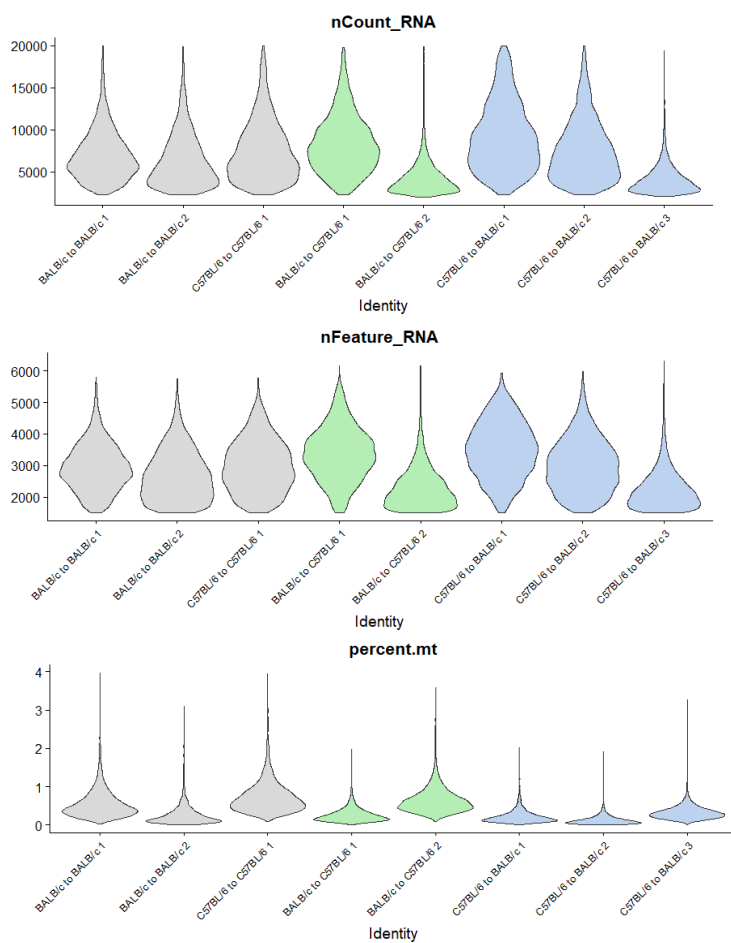
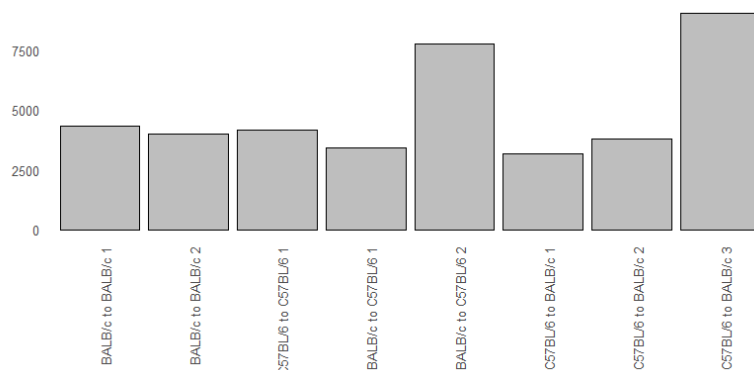
Supplemental Figure S1: Sample information and histology of mouse kidneys from syngeneic and allogeneic groups. A. Sample information for mouse kidney samples. **B.** Representative periodic acid-Schiff (PAS) stained images of the BALB/c and C57BL/6 kidney

isografts and the kidney allografts BALB/c to C57BL/6, C57BL/6 to BALB/c at post-operative day 7, showing interstitial inflammation (red arrows) and tubulitis (black arrows). Note that part of the C57BL/6 to BALB/c allograft is depicted in Fig. 1 in the main body. Scale bar: 50 μ m.



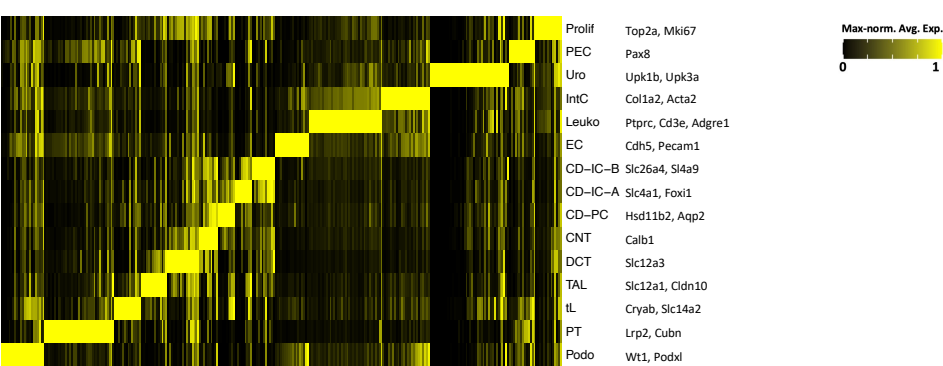
Supplemental Figure S2: Serum urea measurements from syngeneic and allogeneic mice.

Data were analyzed using the Kruskal–Wallis test followed by Dunn’s multiple comparisons test ($n = 3$). Adjusted P -value: $* < 0.05$. Source data are provided as a Source Data file.

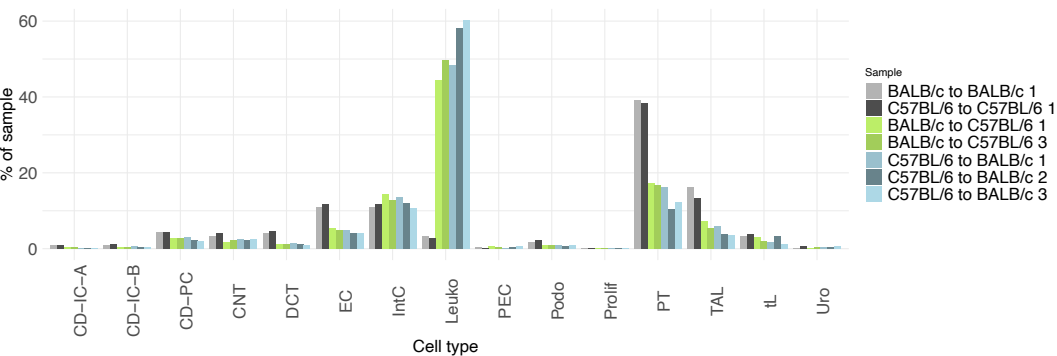
A**B**

Supplemental Figure S3: Quality metrics for mouse snRNA-seq data. **A.** Number of detected genes (*nFeature_RNA*), transcripts (*nCount_RNA*) and percentage of mitochondrial reads (*percent.mt*) per sample. **B.** Number of detected cells per sample. Source data are provided as a Source Data file.

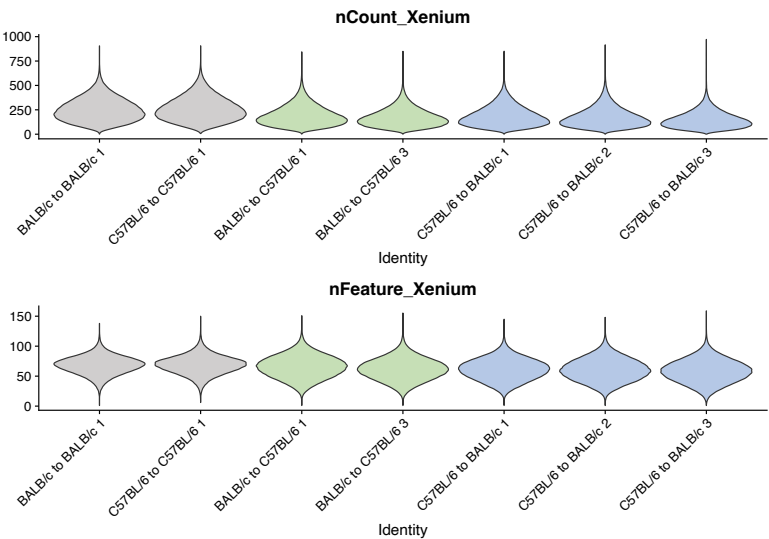
A



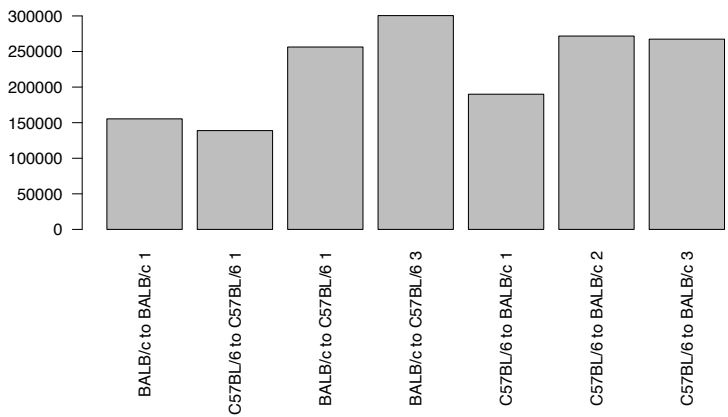
B



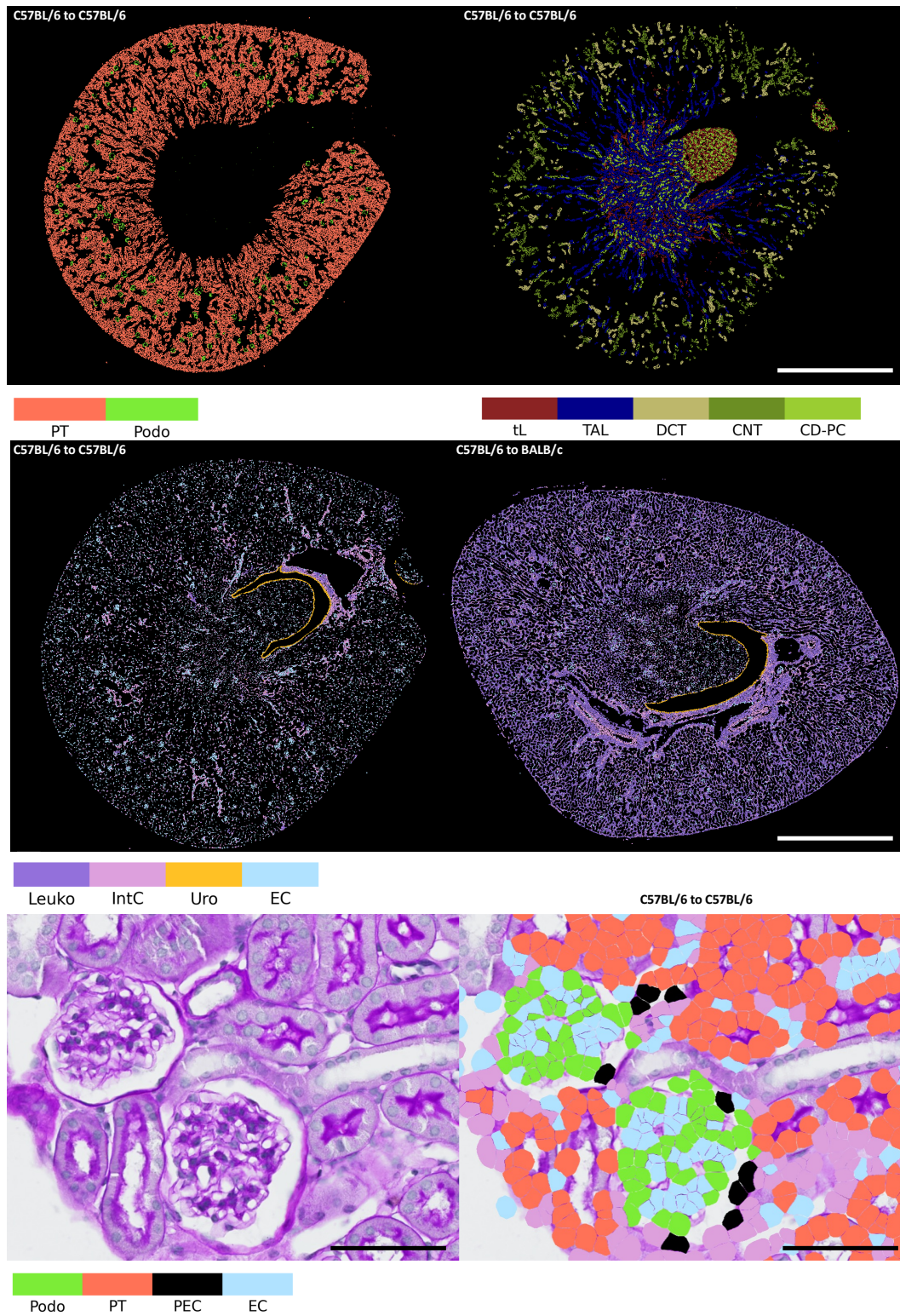
C



D

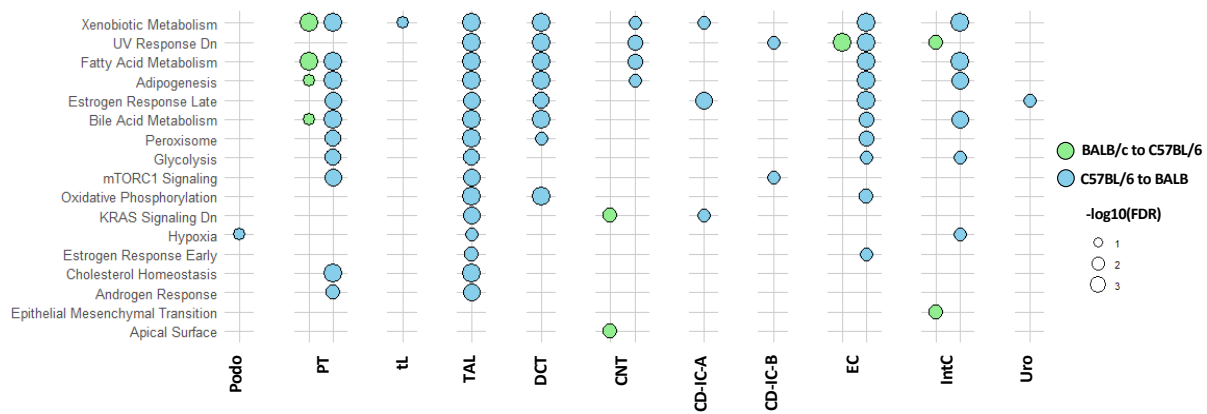
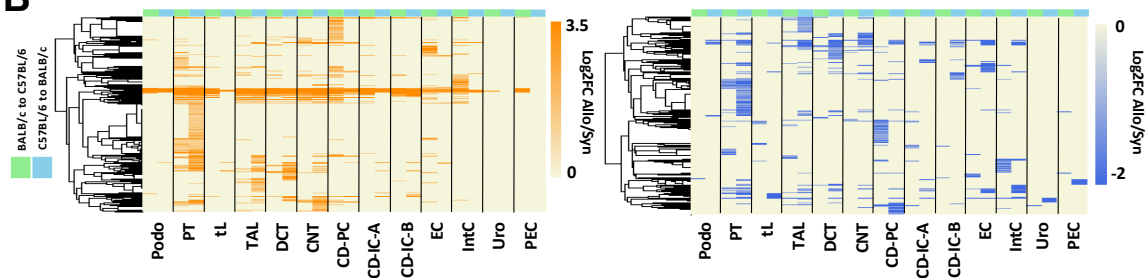


Supplemental Figure S4: Quality metrics and marker gene analysis for mouse ST data. **A.** Broad cell type assignment was performed as detailed in the methods. The heatmap shows marker gene expression, with values normalized to the maximum average expression per gene. Conserved canonical cell type markers shown in the heatmap are displayed to the right of the cell type label. **B.** Relative abundances of major cell types in ST data per sample. **C.** Number of detected genes (*nFeature_Xenium*) and transcripts (*nCount_Xenium*) per sample. **D.** Number of detected and segmented cells per sample. Source data are provided as a Source Data file.



Supplemental Figure S5: Spatial distribution of major cell types. Plots show, as indicated below the respective image, the distribution of major cell types within the kidney as determined

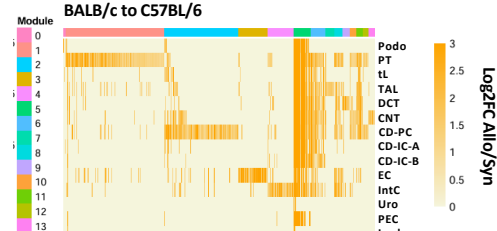
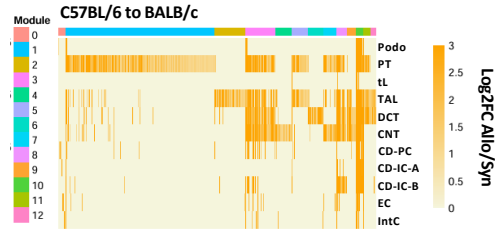
from cell type label transfer from snRNA-seq data. Note the massive infiltration of the rejecting kidney with leukocytes (middle right panel). Modality of transplantation is shown in the upper left corner of the overview images. Scale bar overview: 1000 μ m, scale bar lower images: 50 μ m. All experiments repeated for all spatial transcriptomic samples with similar result.

A**B**

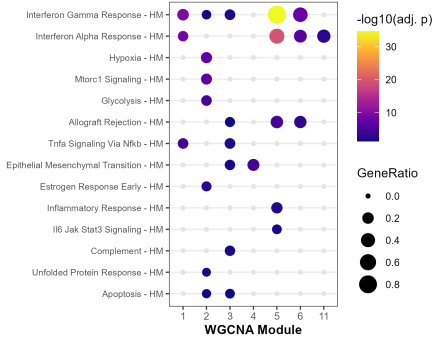
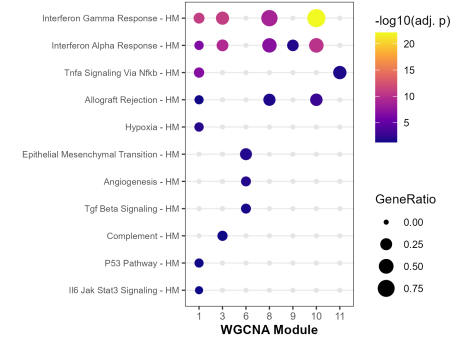
Supplemental Figure S6: Pathway enrichment analysis of differentially regulated genes. A.

Dot plot of pathway enrichment analysis of differentially downregulated genes for each major cell type and transplant group, e.g. BALB/c to C57BL/6 (green) and C57BL/6 to BALB/c (blue). Shown are all significant pathways ($\text{FDR} < 0.05$) from gene set enrichment analysis using hallmark gene sets. **B.** Heatmaps displaying differentially upregulated (left) and downregulated (right) genes by cell type for both groups. Heatmaps show \log_2 fold changes of allogeneic kidneys compared to their respective syngeneic controls. Source data are provided as a Source Data file.

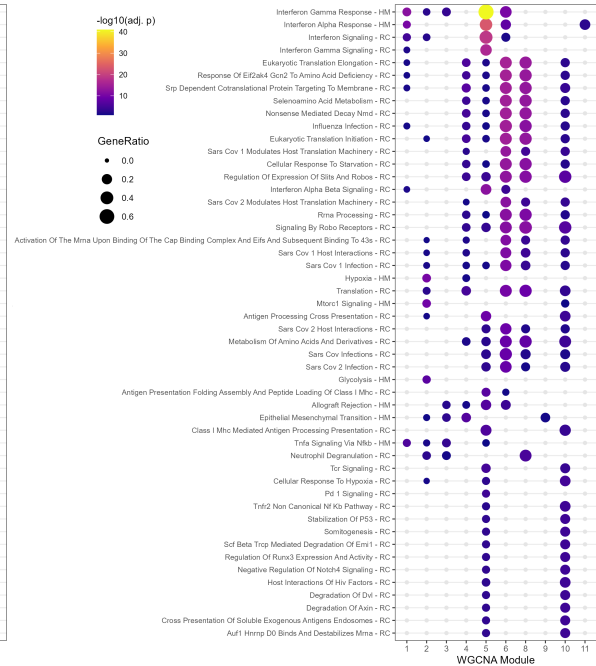
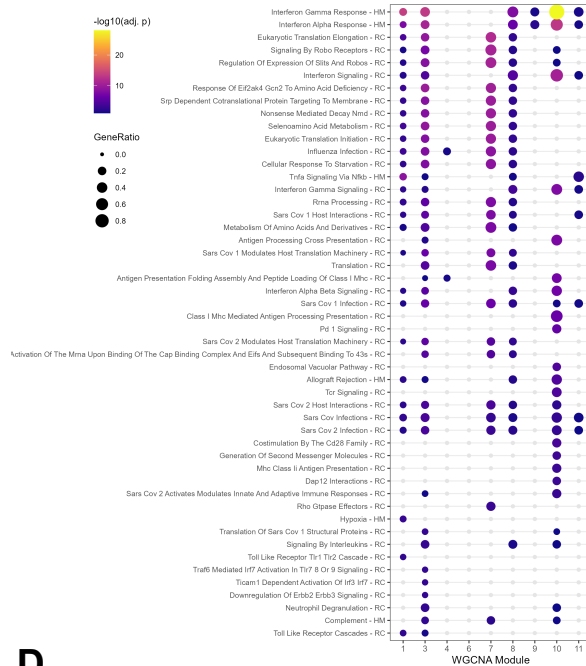
A



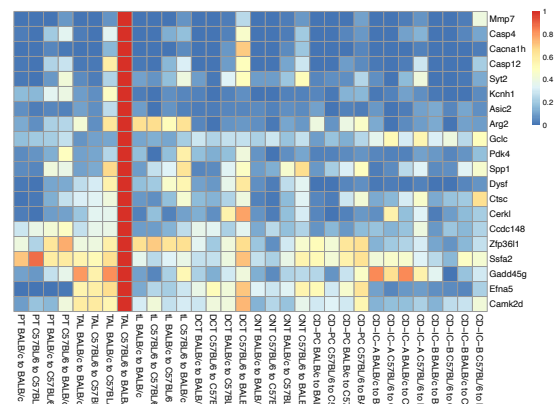
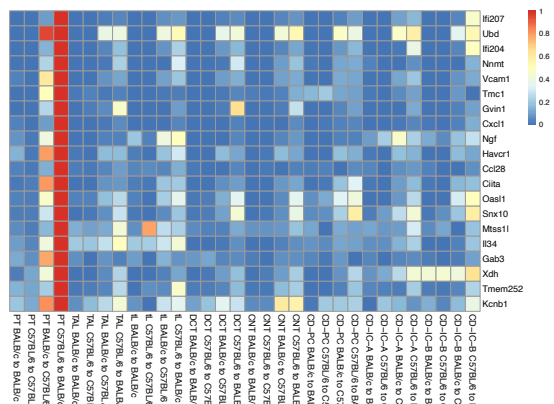
B



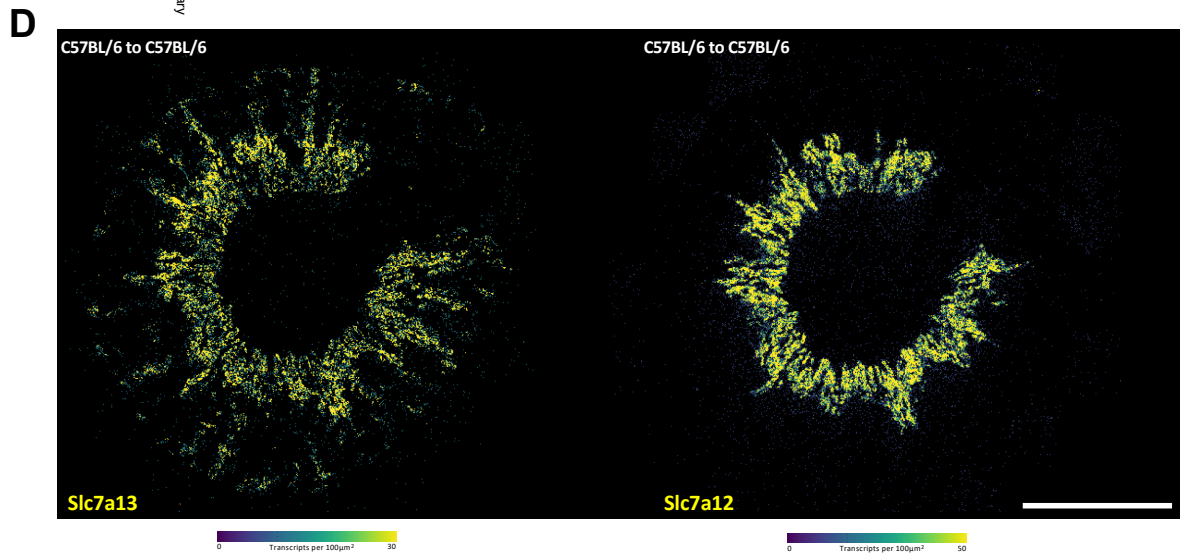
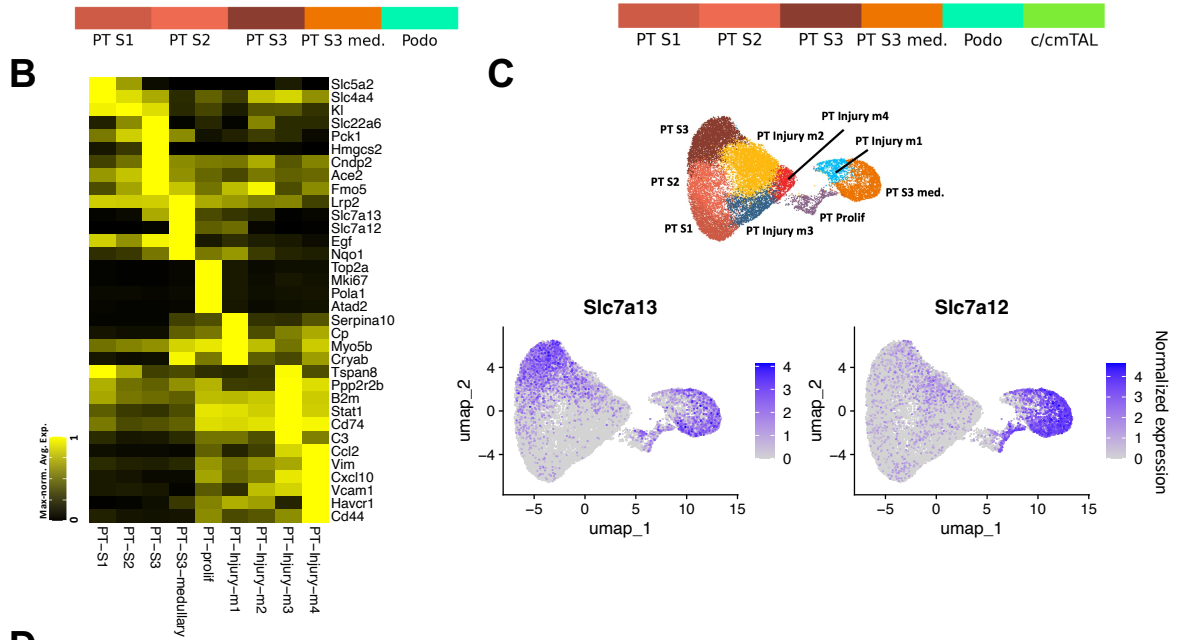
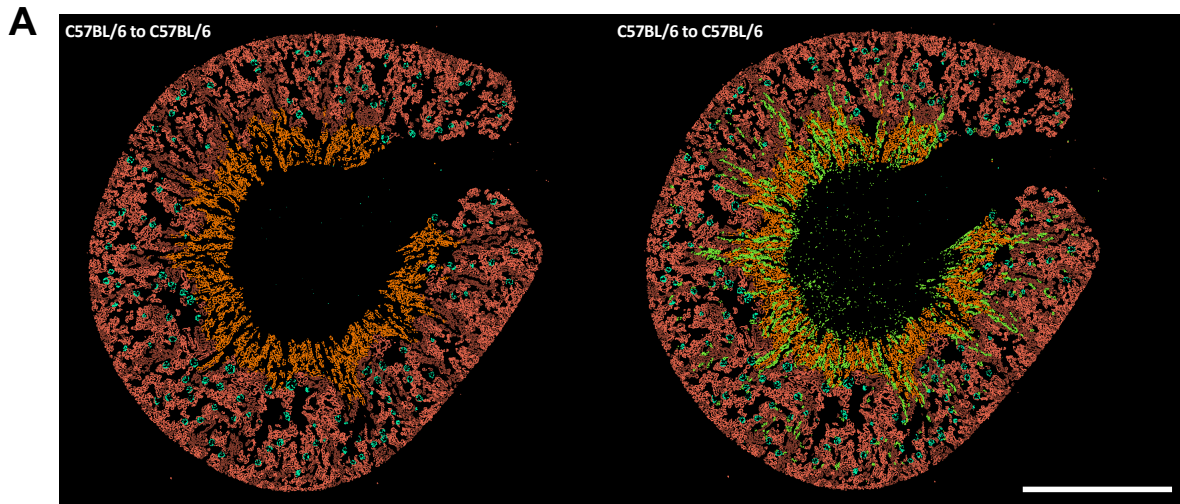
C



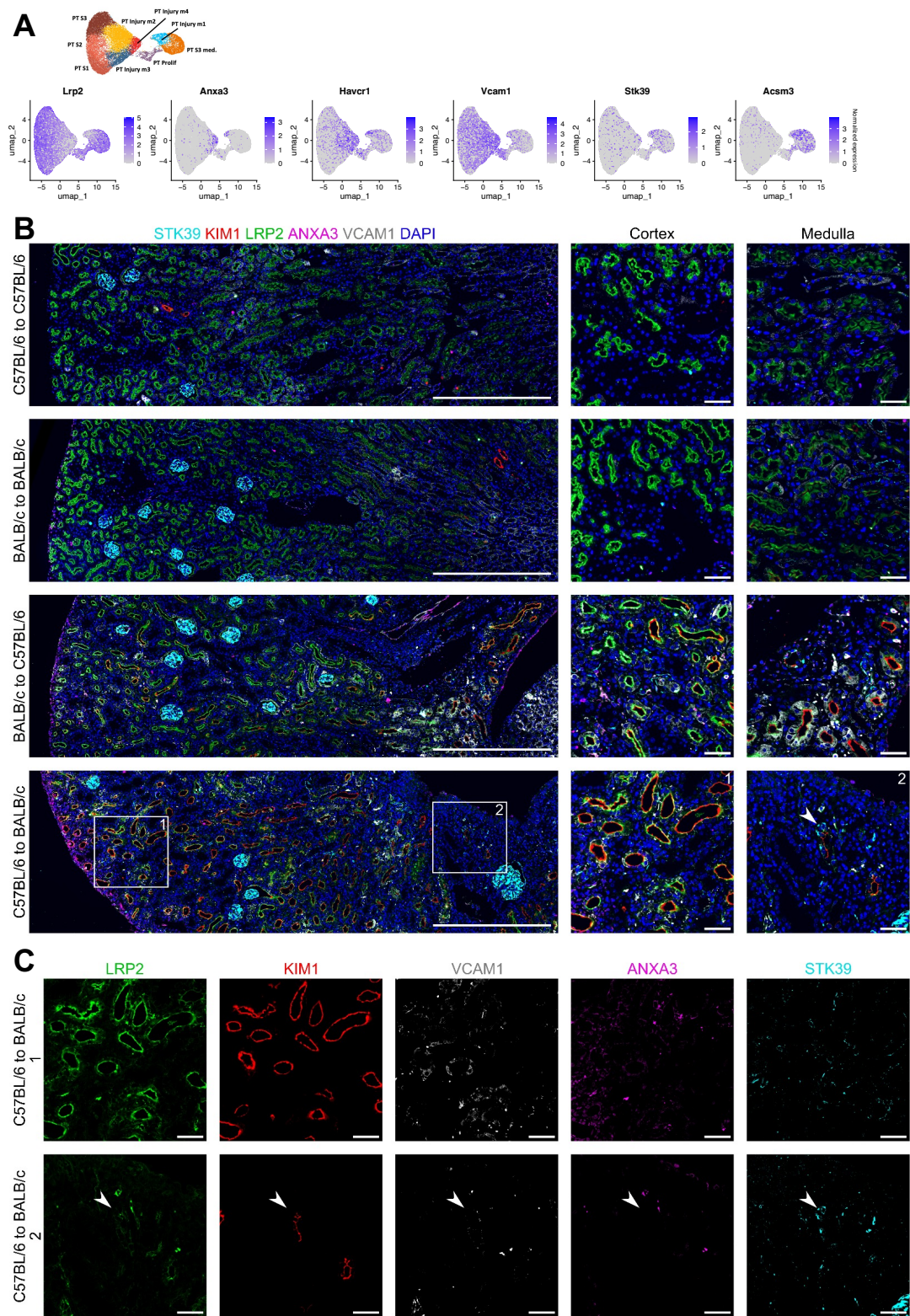
D



Supplemental Figure S7: Analysis of cell type-specific modules and top differentially upregulated genes. **A.** Heatmaps showing the distribution of differentially expressed genes (DEGs with same parameters as in Figure 2) across kidney cell types. Gene co-expression modules were defined using Weighted Gene Correlation Network Analysis (WGCNA) and are displayed with log2 fold-change (allogeneic samples versus respective syngeneic samples) from the DEG analysis. **B.** Hallmark pathway enrichment ($q < 0.05$) per WGCNA module. Dot color indicates $-\log_{10}(\text{adjusted } p\text{-value})$ and dot size reflects the gene ratio. **C.** Hallmark and Reactome pathway enrichment ($q < 0.1$) per WGCNA module, displayed as in B. to include more pathways. **D.** Heatmaps of top differentially upregulated genes in PT and TAL C57BL/6 to BALB/c versus C57BL/6 to C57BL/6. Source data are provided as a Source Data file.

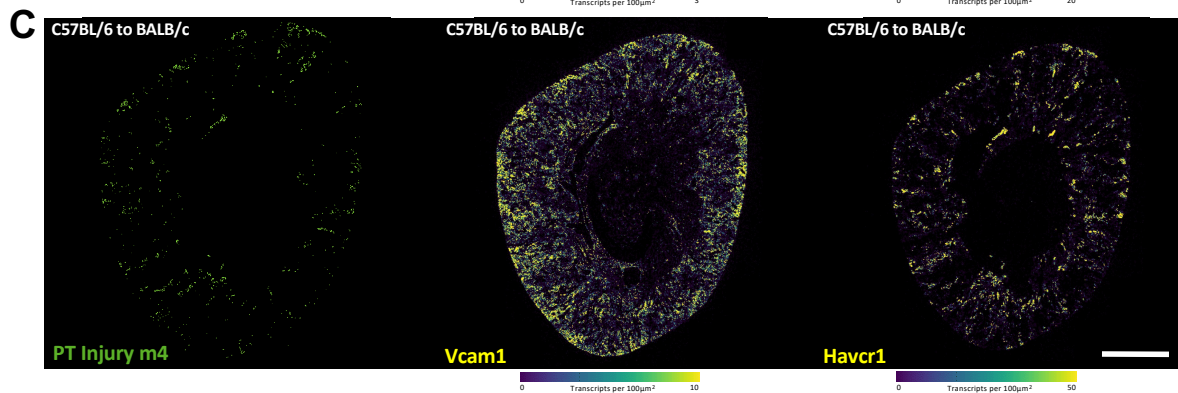
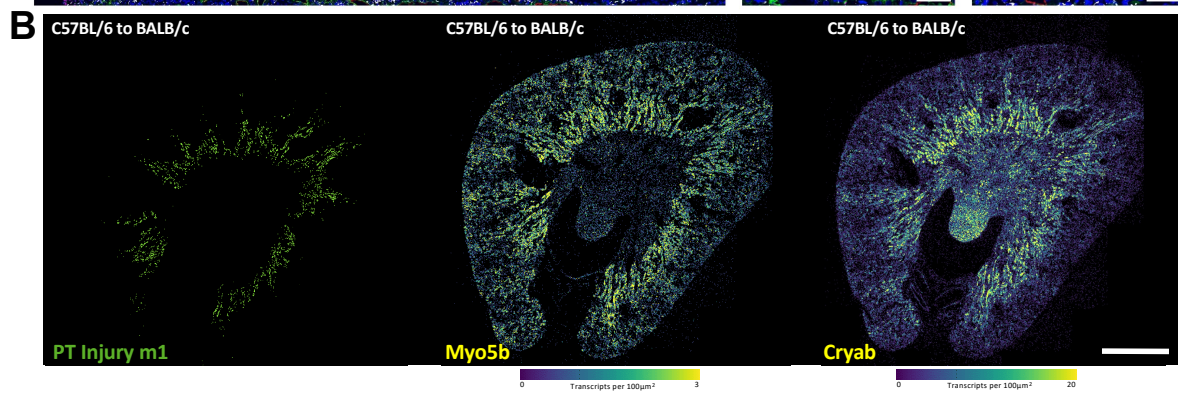
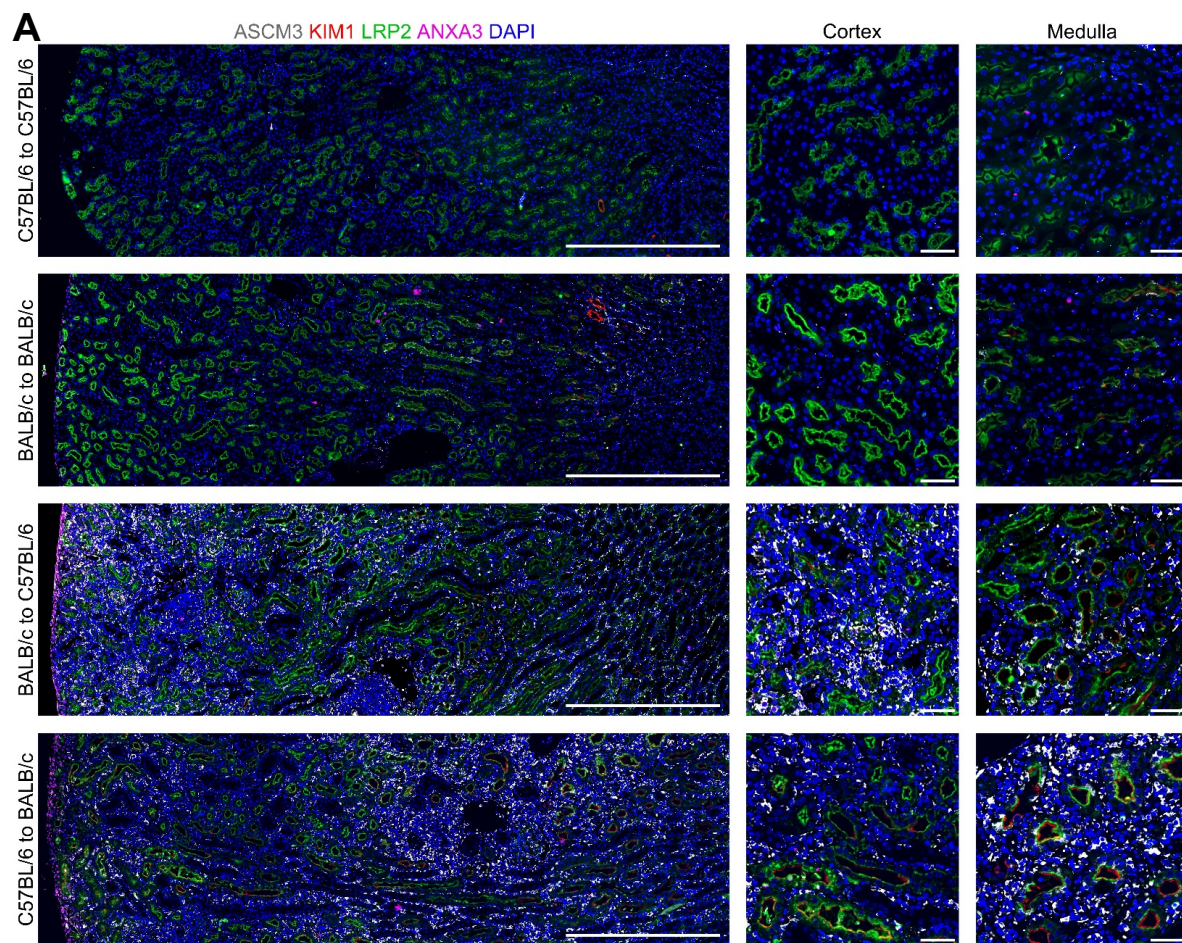


Supplemental Figure S8: Spatial distribution of healthy PT segments from snRNA-seq label transfer. **A.** Distribution of PT subtypes obtained by SingleR-based label transfer from snRNA-seq data. Podocytes are included to facilitate identification of the kidney cortex. While cells from the S3 medullary cluster localize strictly to the medulla, cells from the S3 cluster extend into the medullary rays reaching into the cortex. This visual impression is further emphasized by highlighting cortical and corticomedullary TAL segments in the right panel. **B.** Expression of snRNA-seq-derived PT marker genes in spatial transcriptomics data (see Fig. 3 for expression in snRNA-seq data). **C.** Feature plots of the S3 and S3 medullary marker gene *Slc7a13* and the S3 medullary marker gene *Slc7a12* in PT cells from snRNA-seq data. **D.** Transcript density plots for *Slc7a12* and *Slc7a13*. Spatial distribution of S3 and S3 medullary cells corresponds closely to the expression domains of *Slc7a13* and *Slc7a12* in ST data as expected from label transfer and snRNA-seq data (compare to A.). Transcript densities are represented according to the color scale. Scale bar: 1000 μ m. Source data are provided as a Source Data file. All experiments repeated for all spatial transcriptomic samples with similar result.



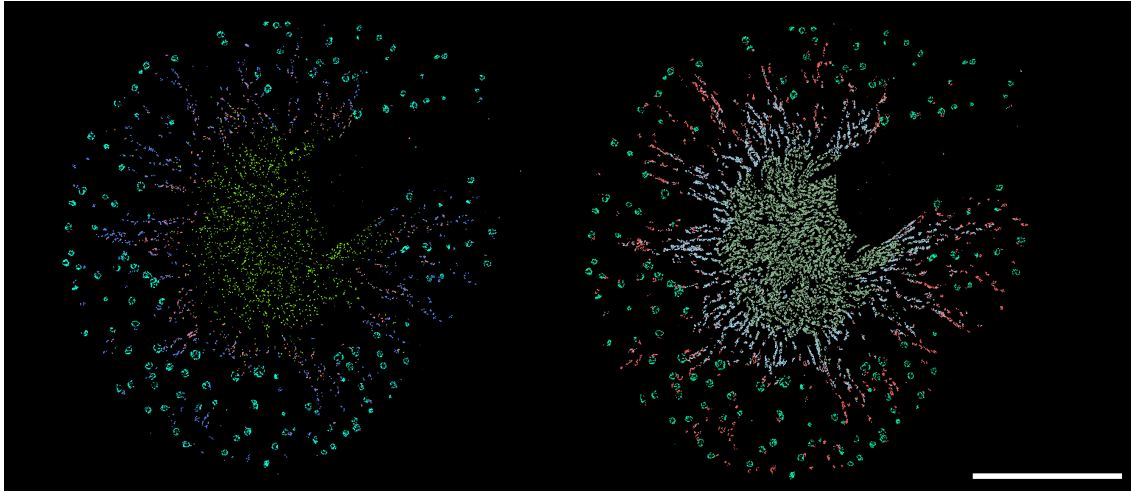
Supplemental Figure S9: Validation of PT Injury m1 and m4. **A.** Feature plots of PT cells from mouse snRNA-seq data showing expression of PT Injury m4 marker genes (Anxa3, Havcr1,

Vcam1) and PT Injury m1 marker genes (*Stk39*, *Acsn3*; medullary injury cluster) as well as canonical PT marker gene *Lrp2*. Expression domains partially overlap, with PT Injury m4 markers also showing expression within the PT Injury m1 domain. **B.** Immunofluorescence staining for *STK39*, *VCAM1*, *ANXA3* and *KIM1* (encoded by *Havcr1*) in syngeneic and allogeneic mouse kidneys. In allogeneic kidneys, *STK39* (cyan) shows distinct medullary proximal tubule expression, often separated from the *VCAM1* (white) domain. *ANXA3* (magenta) overlaps with *KIM1* (red) but not with *STK39*. All marker signals co-localize with the canonical proximal tubule marker *LRP2* (green). Comparative analysis with syngeneic kidneys confirms the specificity and spatial distribution of marker expression. Scale bars: 500 μm (large image); 50 μm (cortex and medulla). All experiments repeated three times with similar result. **C.** Single-channel images of the stained markers in allogeneic transplanted kidneys (C57BL/6 to BALB/c) show conserved spatial localization and marker co-expression in cortical (1) and medullary (2) regions. Nuclei are counterstained with DAPI. Scale bar: 50 μm .



Supplemental Figure S10: Validation of PT Injury m1 and m4. **A.** Immunofluorescence staining for the PT Injury m1 marker ACSM3 and PT Injury m4 markers ANXA3 and KIM1 (HAVCR1), together with the canonical PT marker LRP2. Expression domains partially overlap, as shown in the feature plots (Supplementary Fig. S9A). PT Injury m4 markers also display some expression within the PT Injury m1 domain. In allogeneic mouse kidneys, ACSM3 (white) shows distinct expression in medullary proximal tubules, demonstrated by co-localization with LRP2 (green). ACSM3-positive cells are predominantly positive for KIM1 (red) but negative for ANXA3 (magenta). Nuclei are counterstained with DAPI. Scale bars: 500 μm (large image); 50 μm (cortex and medulla). All experiments repeated three times with similar result. **B.** Gene density plots for PT Injury m1 marker genes *Myo5b* and *Cryab*, and **C.** for PT Injury m4 marker genes *Vcam1* and *Havcr1* from spatial transcriptomics data. Scale bar: 1000 μm . Transcript densities are represented according to the color scale. Left panels depict the spatial localization of PT Injury m1 and m4 cell populations as inferred from snRNA-seq label transfer, respectively. All experiments repeated for all allogeneic spatial transcriptomic samples with similar result.

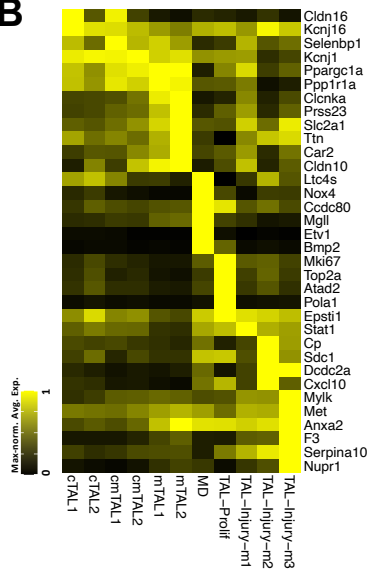
A



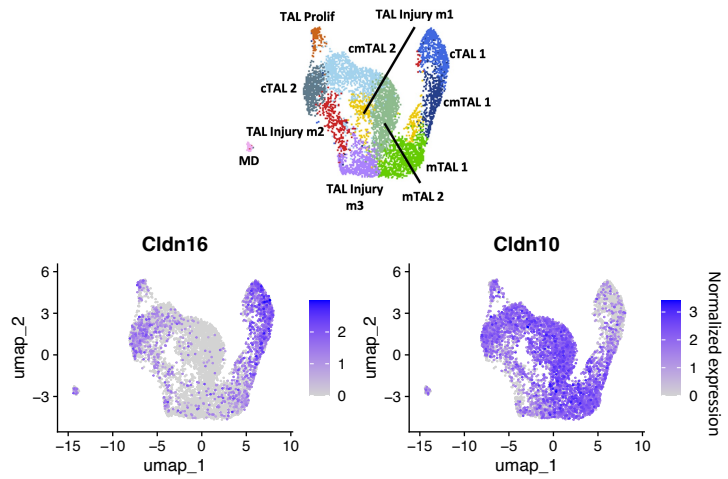
cTAL1 cmTAL1 mTAL1 Podo

cTAL2 cmTAL2 mTAL2 Podo

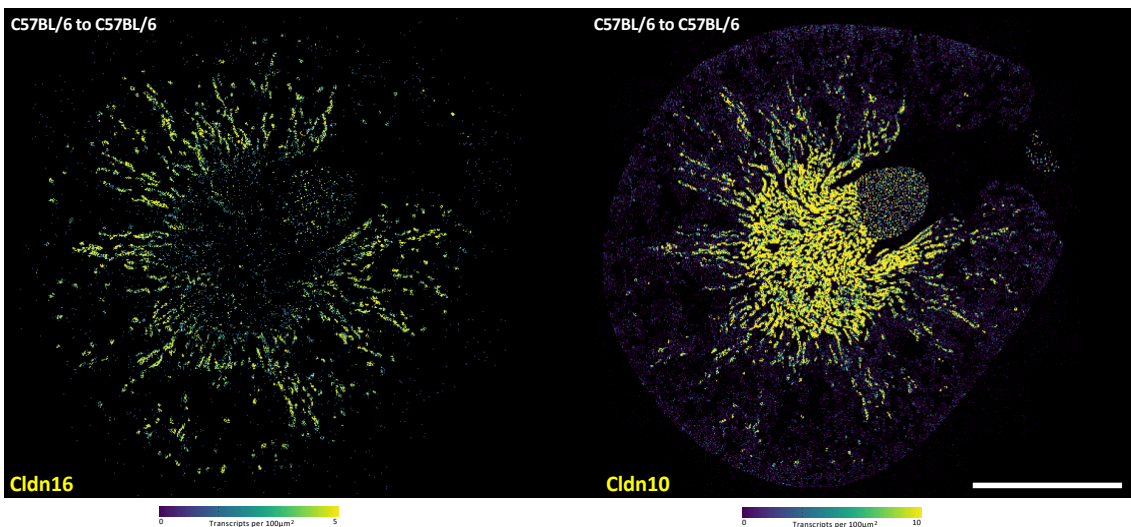
B



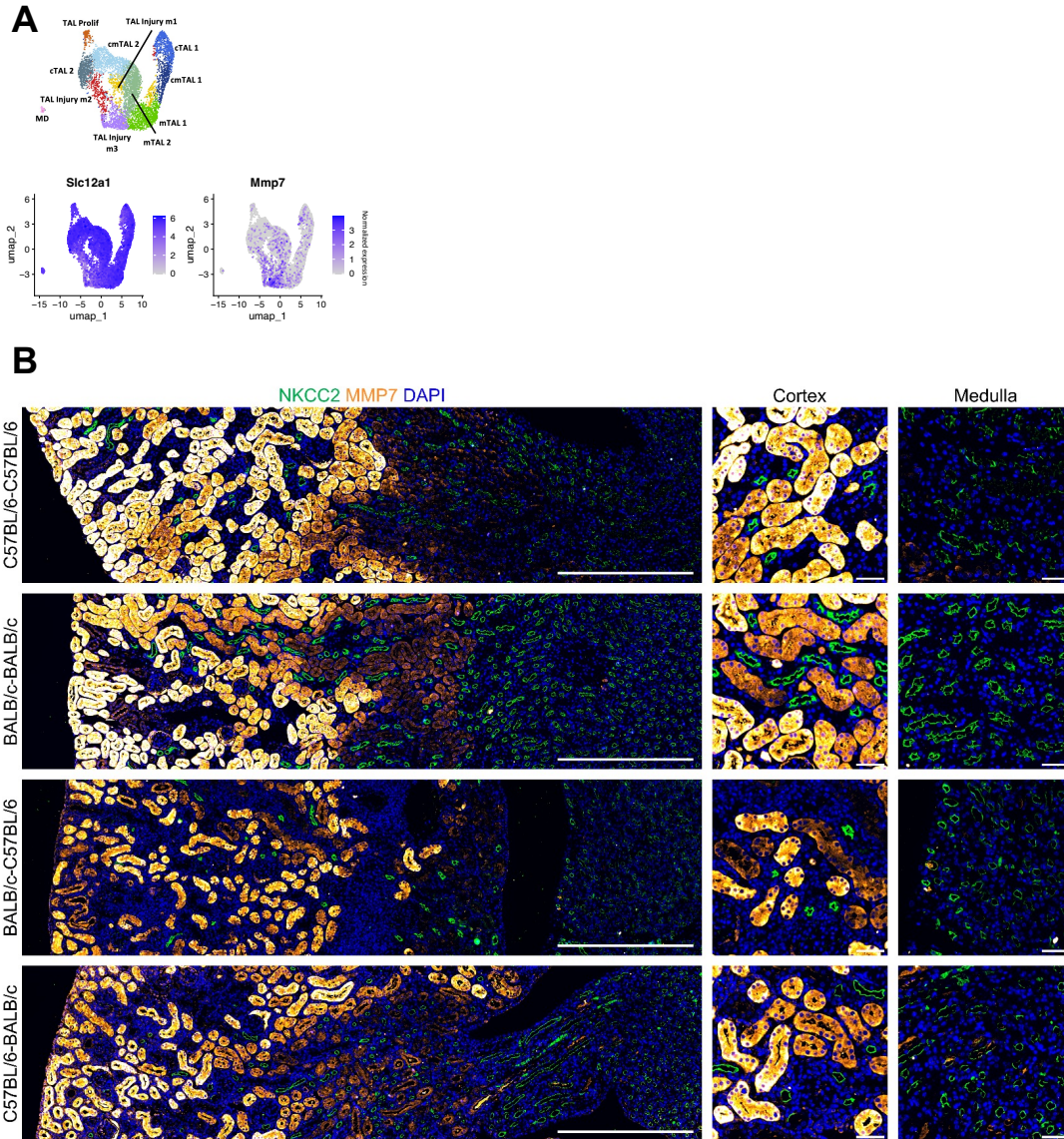
C



D

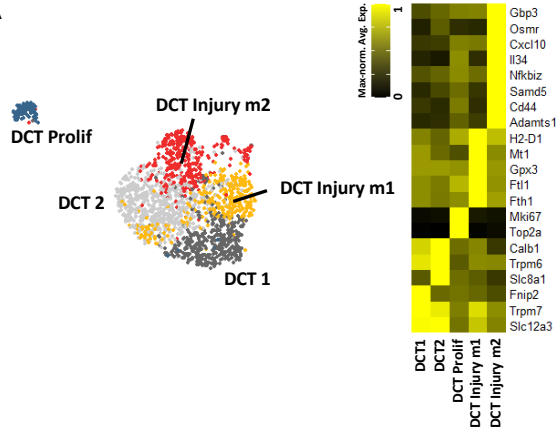


Supplemental Figure S11: Spatial distribution of healthy TAL segments from snRNA-seq label transfer. **A.** Distribution of TAL subtypes obtained by SingleR-based label transfer from snRNA-seq data. Podocytes are included to facilitate identification of the kidney cortex. cTAL1 and cmTAL1 show elevated Cldn16 expression (with very residual expression in mTAL1) while cTAL2, cmTAL2 and mTAL2 are predominantly expressing Cldn10. All experiments repeated for all spatial transcriptomic samples with similar result. **B.** Expression of snRNA-seq-derived TAL marker genes in spatial transcriptomics data (see Fig. 3 for expression in snRNA-seq data). **C.** Feature plots of the mentioned claudins, Cldn10 and Cldn16 in TAL cells from snRNA-seq data. **D.** Transcript density plots for Cldn16 and Cldn10 reflecting the mentioned cTAL1-cmTAL1-mTAL1 and cTAL2-cmTAL2-mTAL2 axes. Transcript densities are represented according to the color scale. Scale bar: 1000 μm . Source data are provided as a Source Data file. All experiments repeated for all spatial transcriptomic samples with similar result.

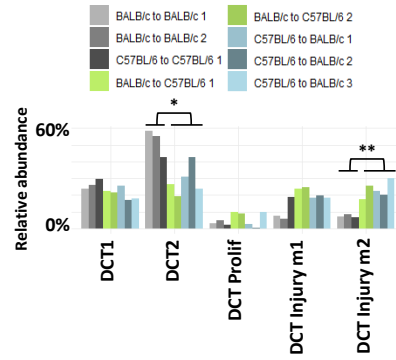


Supplemental Figure S12: Validation of TAL Injury m3. **A.** Feature plots of TAL cells from mouse snRNA-seq data showing expression of TAL Injury m3 marker gene *Mmp7* as well as canonical TAL marker gene *Slc12a1*. **B.** Immunofluorescence staining for MMP7. Within the TAL, the TAL Injury m3 marker MMP7 is expressed in scattered medullary NKCC2-positive TAL cells in allogeneic transplanted kidneys but is absent in syngeneic grafts (*Slc12a1* encodes NKCC2). The predominant medullary localization of TAL Injury m3 was anticipated from label transfer of snRNA-seq data to the spatial transcriptomics dataset (see Fig. 3G). Nuclei are counterstained with DAPI. MMP7 also labels PT cells. The lower panels, also shown in Fig. 3J, are reproduced here for convenience. Scale bars: 500 μm (large image); 50 μm (cortex and medulla). All experiments repeated three times with similar result.

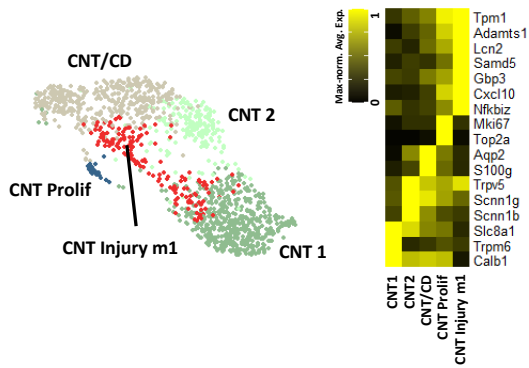
A



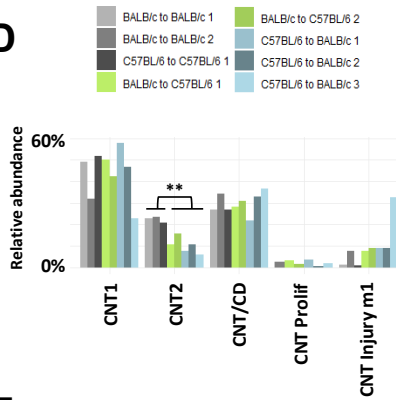
B



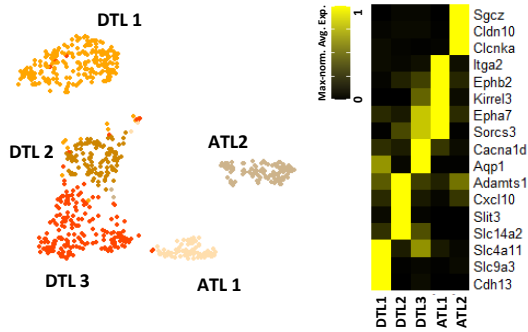
C



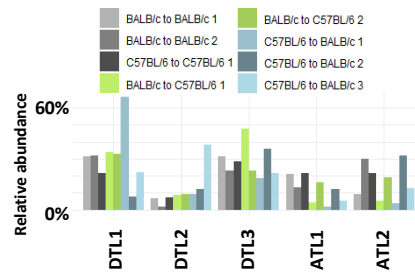
D



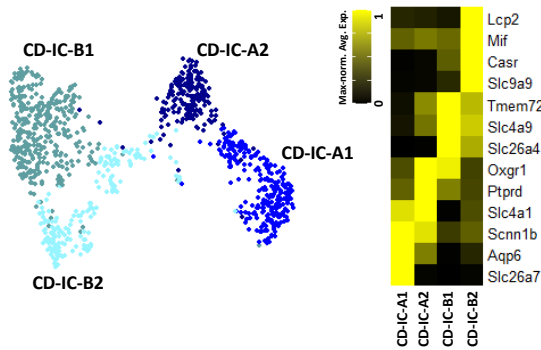
E



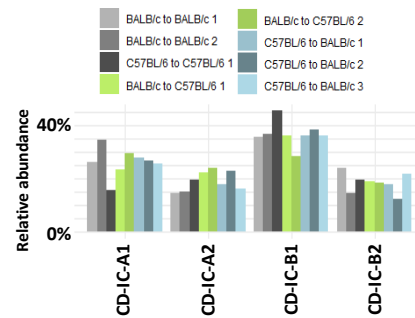
F



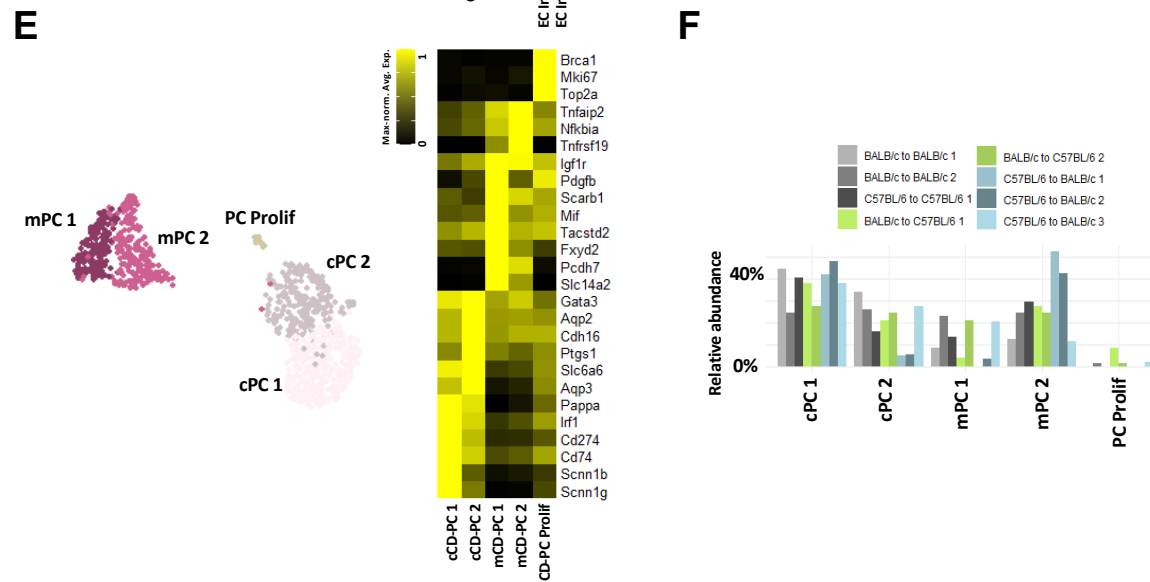
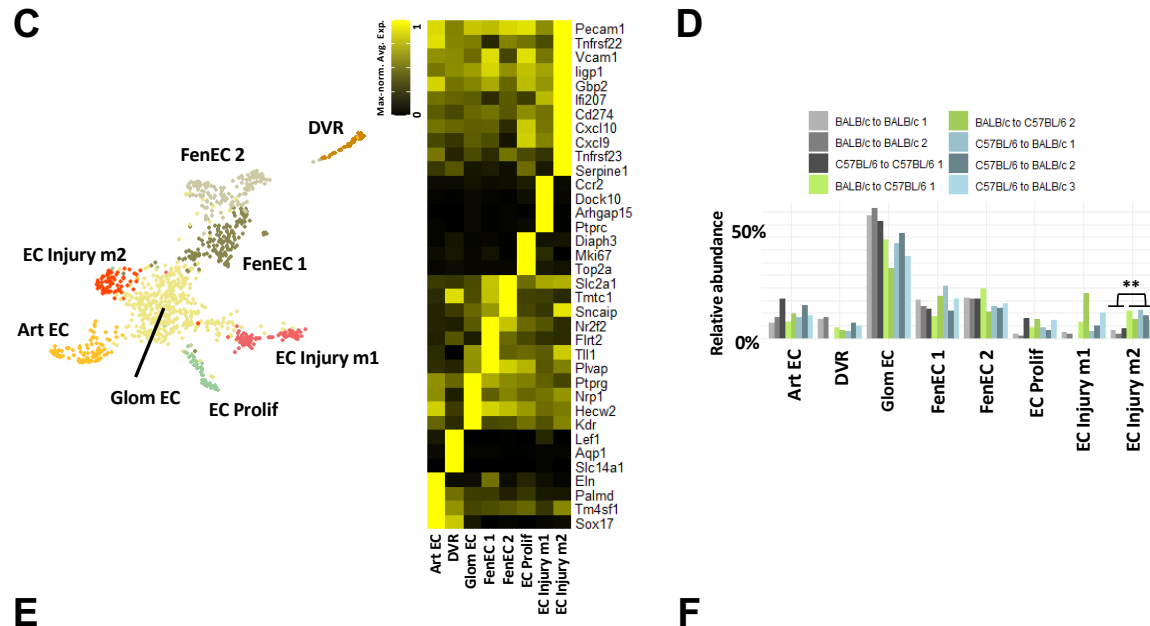
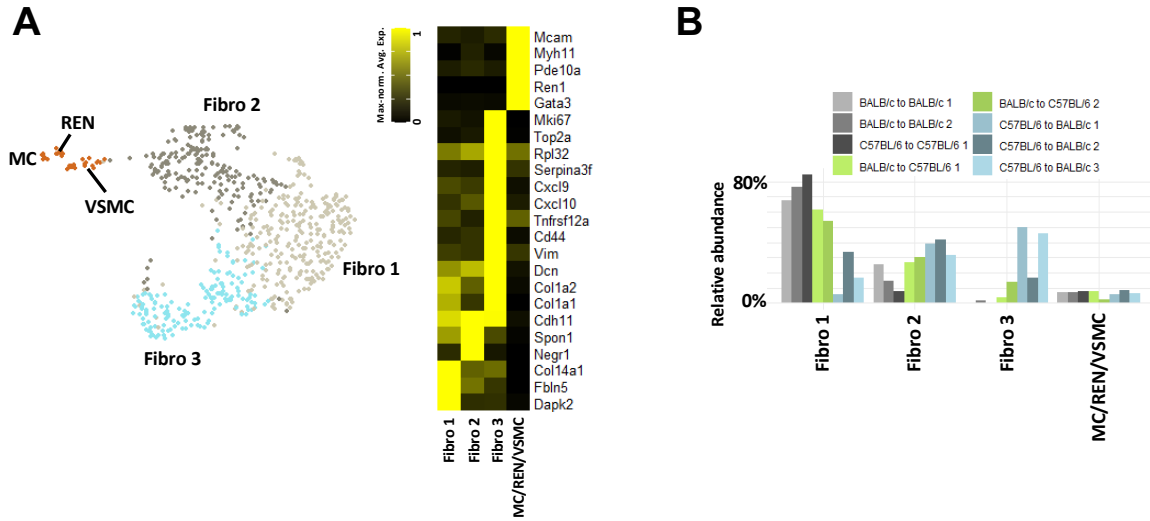
G



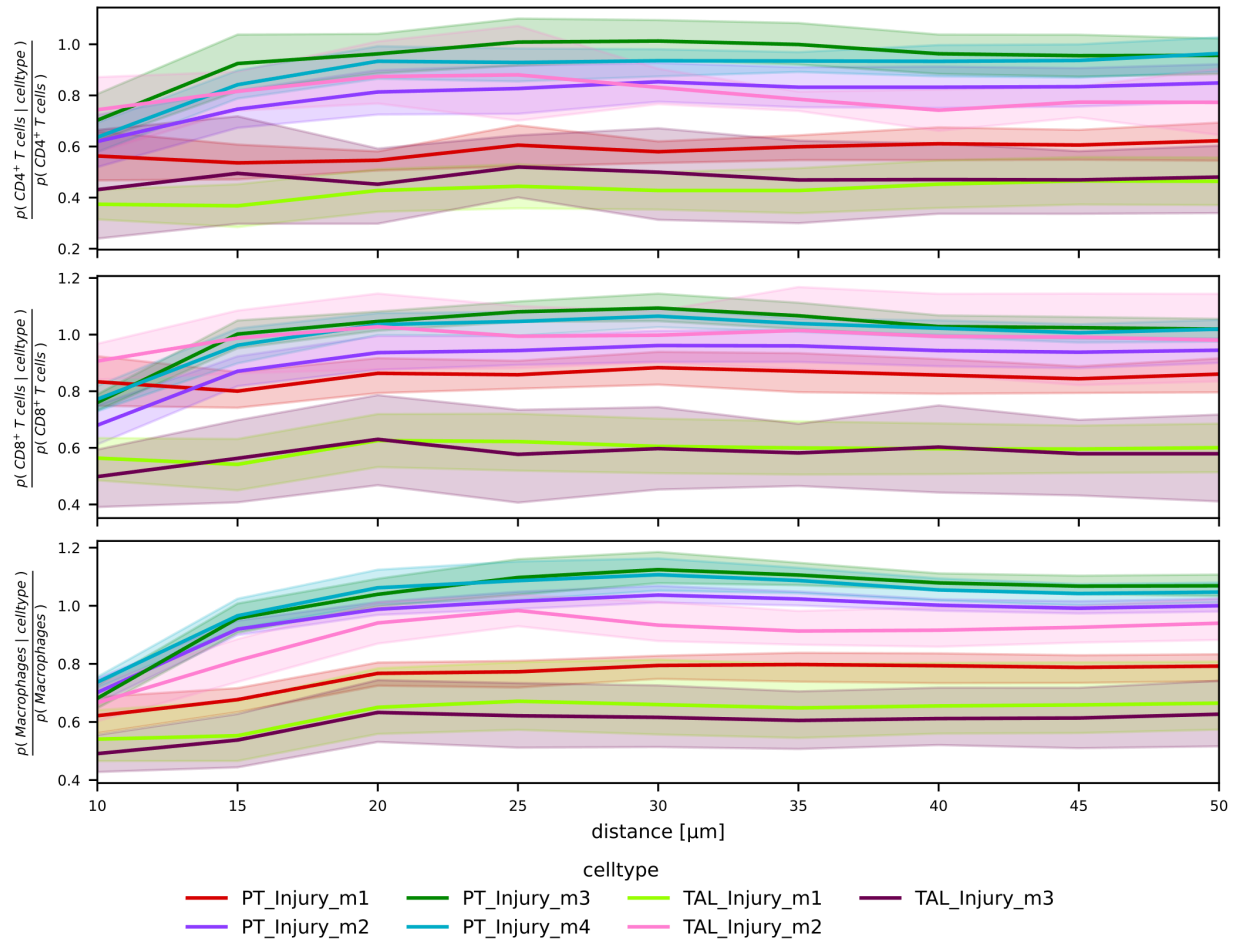
H



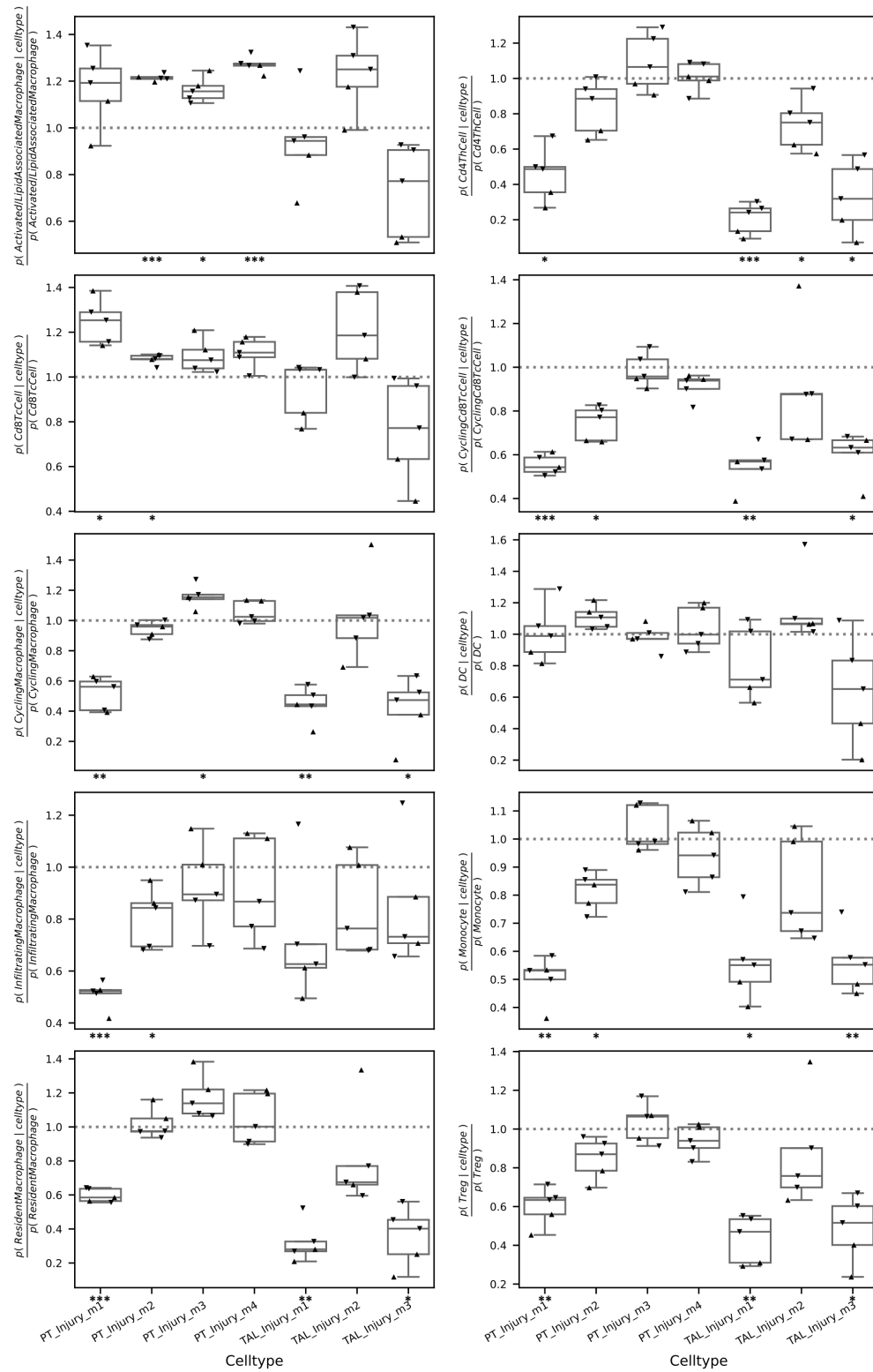
Supplemental Figure S13: Results from subclustering analysis of remaining major cell types. Note that subclustering of leukocytes is included in the main figures. Analyses as indicated for DCT (**A.** and **B.**), CNT (**C.** and **D.**), TL (**E.** and **F.**, ATL – ascending thin limb, DTL – descending thin limb) and CD-IC (**G.** and **H.**). Heatmaps show marker gene expression (counts per million, maximum-normalized per gene). Student's *t*-test with Benjamini-Hochberg correction for multiple testing. *P*-value: * <0.05 , ** <0.005 , no asterisk – not significant. Source data are provided as a Source Data file.



Supplemental Figure S14: Results from subclustering analysis of remaining major cell types. Note that subclustering leukocytes is included in the main figures. Analyses as indicated for interstitial cells (**A.** and **B.**, MC – mesangial cells, REN – renin-producing cells, VSMC – vascular smooth muscle cells, Fibro - fibroblasts), EC (**C.** and **D.**, FenEC – fenestrated EC, Glom EC – glomerular EC, Art EC – arterial EC, DVR – descending vasa recta) and CD-PC (**E.** and **F.**, mPC – medullary principal cells, cPC – cortical principal cells). Heatmaps show marker gene expression (counts per million, maximum-normalized per gene). Student's *t*-test with Benjamini-Hochberg correction for multiple testing. *P*-value: **<0.005, no asterisk – not significant. Source data are provided as a Source Data file.

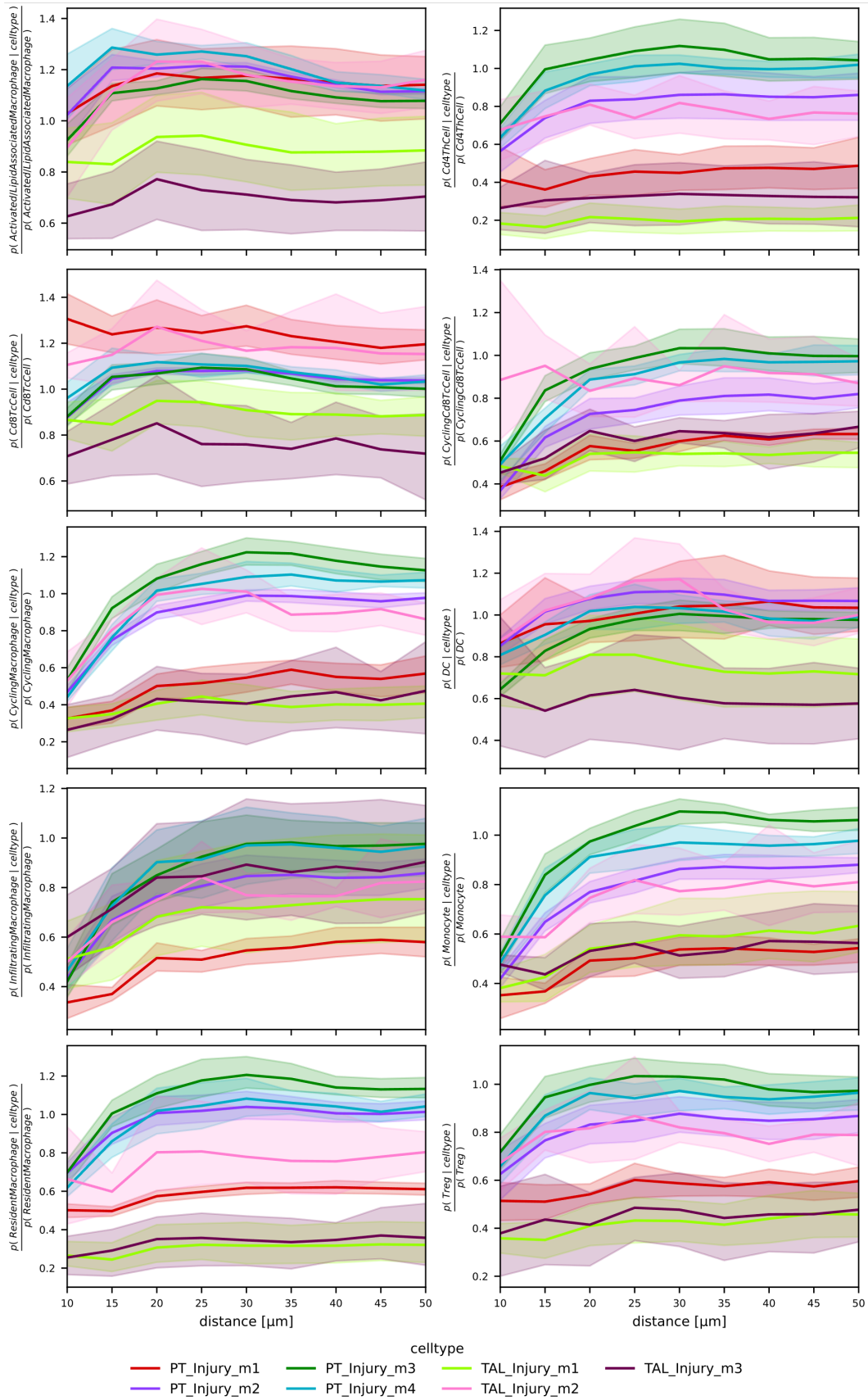


Supplemental Figure S15: Spatial proximity of PT and TAL injury clusters to major immune cell types. For every injury cluster of interest (e.g. PT Injury m4), the co-occurrence to each leukocyte cell type was calculated with squidpy. Briefly, `squidpy.gr.co_occurrence` was run with a distance interval of 10 to 50 μm with step size 5 based on the provided centroid information from the Xenium data. Compare to analysis for 25 μm in Fig. 4E. Source data are provided as a Source Data file.

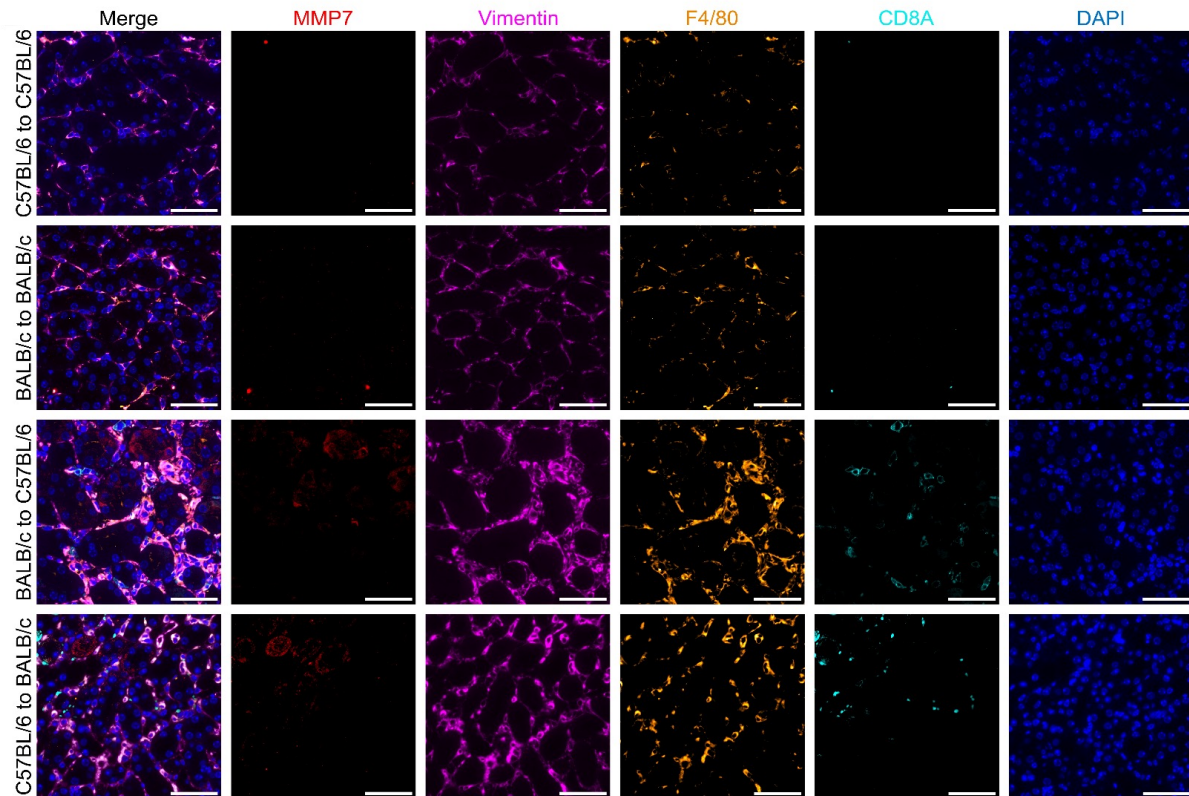


Supplemental Figure S16: Co-occurrence of PT and TAL injury clusters with immune cell cell subtypes. As in Fig. 4E, we chose 25 μm as indicative of being a direct neighbour.

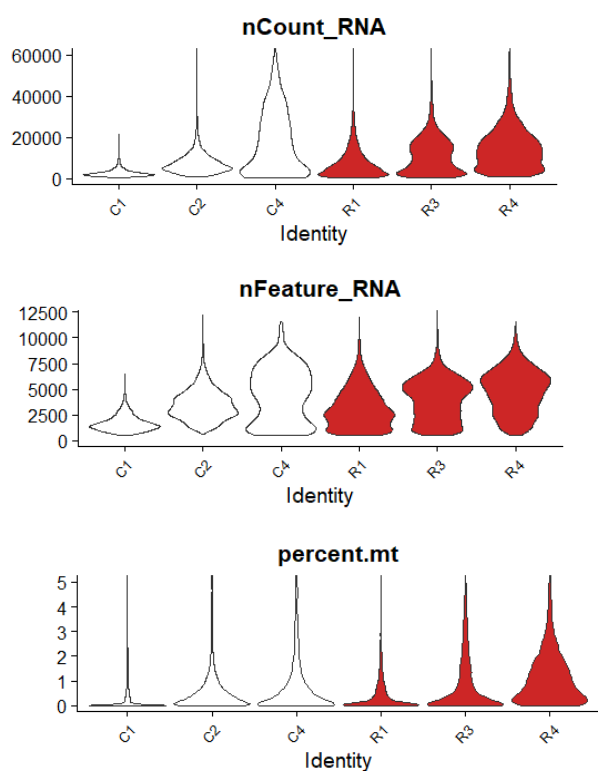
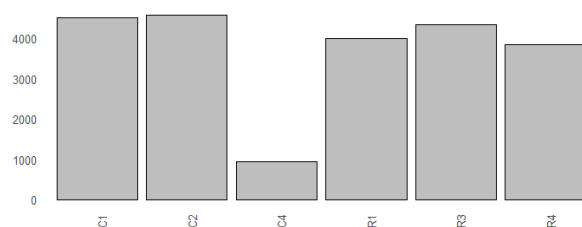
*Significances from statistical testing below individual boxes. Two-sided one sample t-test with Benjamini-Hochberg correction for multiple testing. P-value: * <0.05 , ** <0.005 , *** <0.001 . Source data are provided as a Source Data file. Box plots show the median and the 25th–75th percentiles, with whiskers extending to the most extreme data points within $1.5\times$ the interquartile range. Analogous to Fig. 4E, allogeneic transplantation C57BL/6 to BALB/c (triangles pointing downwards, $n = 3$) and BALB/c to C57BL/6 (triangles pointing upwards, $n = 2$).*



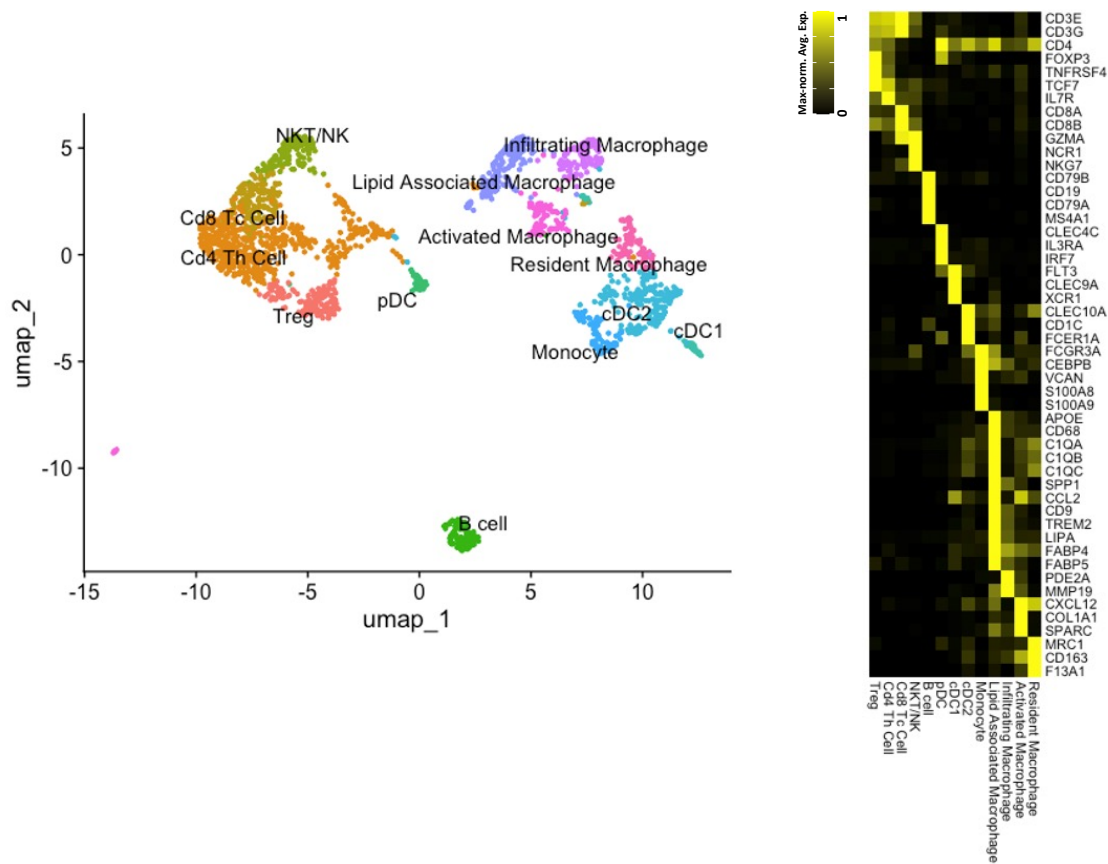
Supplemental Figure S17: Spatial proximity of PT and TAL injury clusters to immune cell subtypes. Figure analogous to Suppl. Fig. S15 for immune cell subtypes. Source data are provided as a Source Data file.



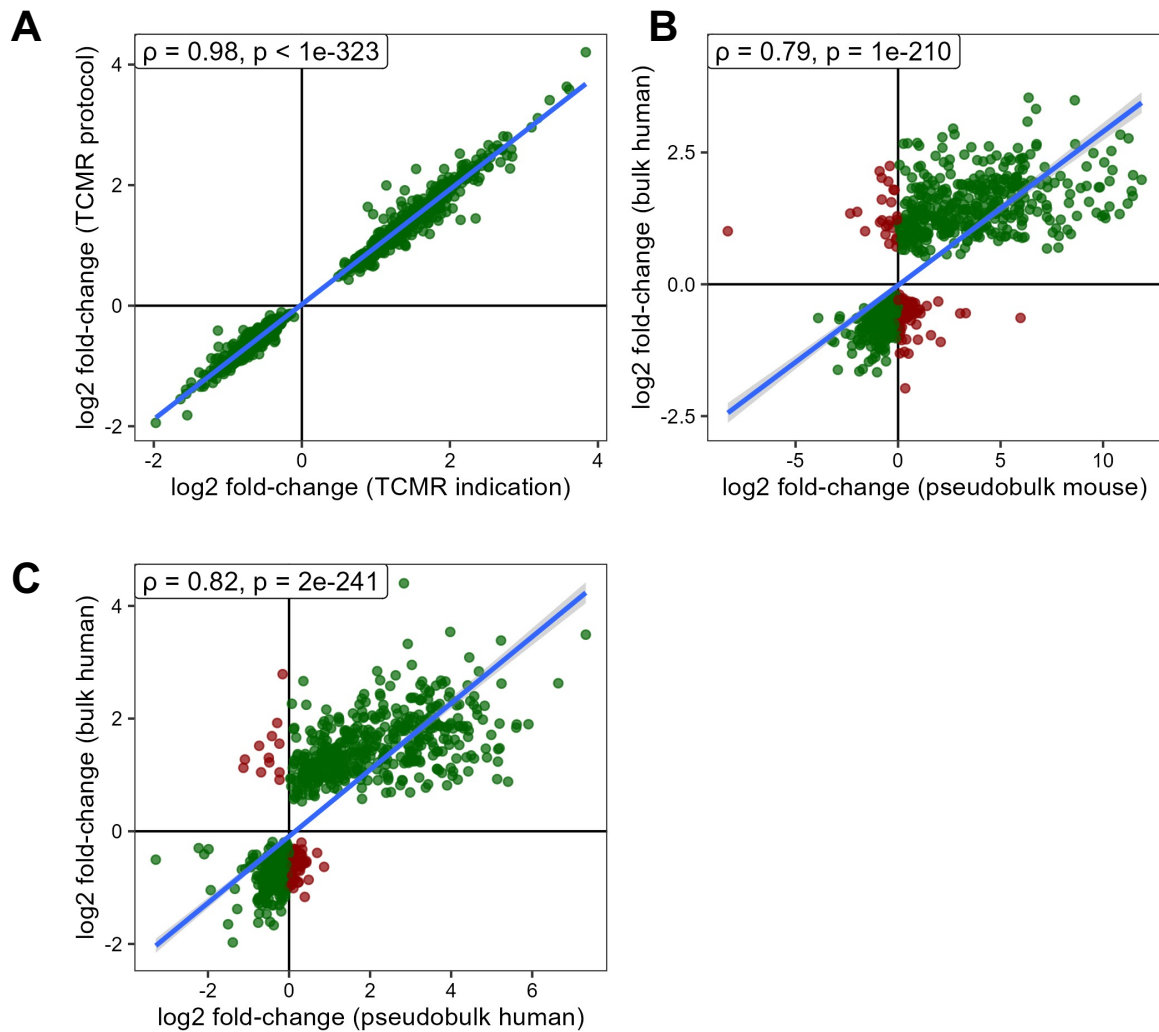
Supplemental Figure S18: Localization of MMP7-positive TAL cells (TAL Injury m3) with fibroblasts, macrophages and CD8A-positive T cells. Immunofluorescence staining for F4/80 (macrophages, orange), CD8A (CD8⁺ T cells, cyan), Vimentin (Vim, fibroblasts and macrophages, magenta) and MMP7 (TAL Injury m3, red). Injured TAL cells show markedly fewer or no direct contacts with immune cells compared to PT Injury m4 (see Fig. 5E). Nuclei are counterstained with DAPI. Scale bar: 50 μ m. All experiments repeated three times with similar result.

A**B**

Supplemental Figure S19: Quality metrics for human snRNA-seq data. A. Number of detected genes (*nFeature_RNA*), transcripts (*nCount_RNA*) and percentage of mitochondrial reads (*percent.mt*) per sample. **B.** Number of detected cells per sample. Source data are provided as a Source Data file.



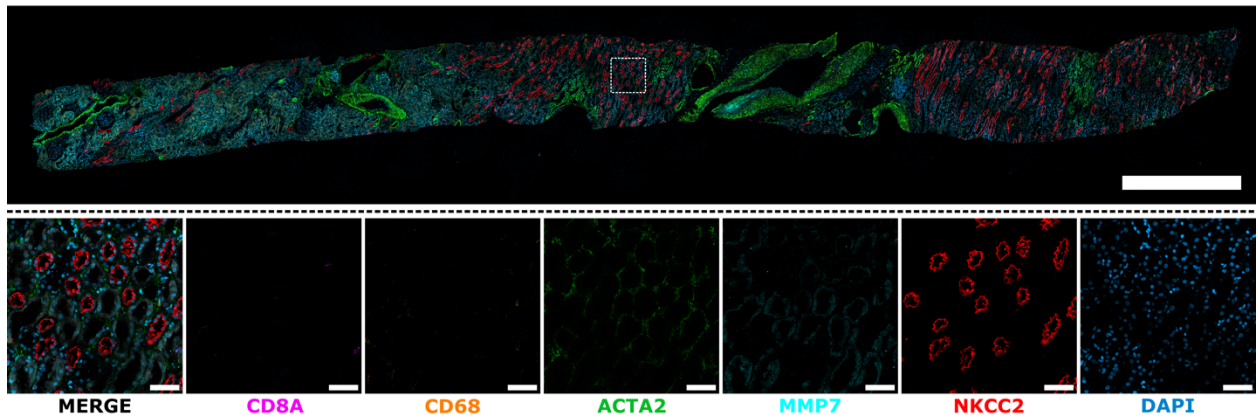
Supplemental Figure S20: Subclustering of human leukocytes. UMAP of human snRNA-seq leukocyte subclustering with marker gene heatmap on the right side (maximum-normalized gene expression). Source data are provided as a Source Data file.



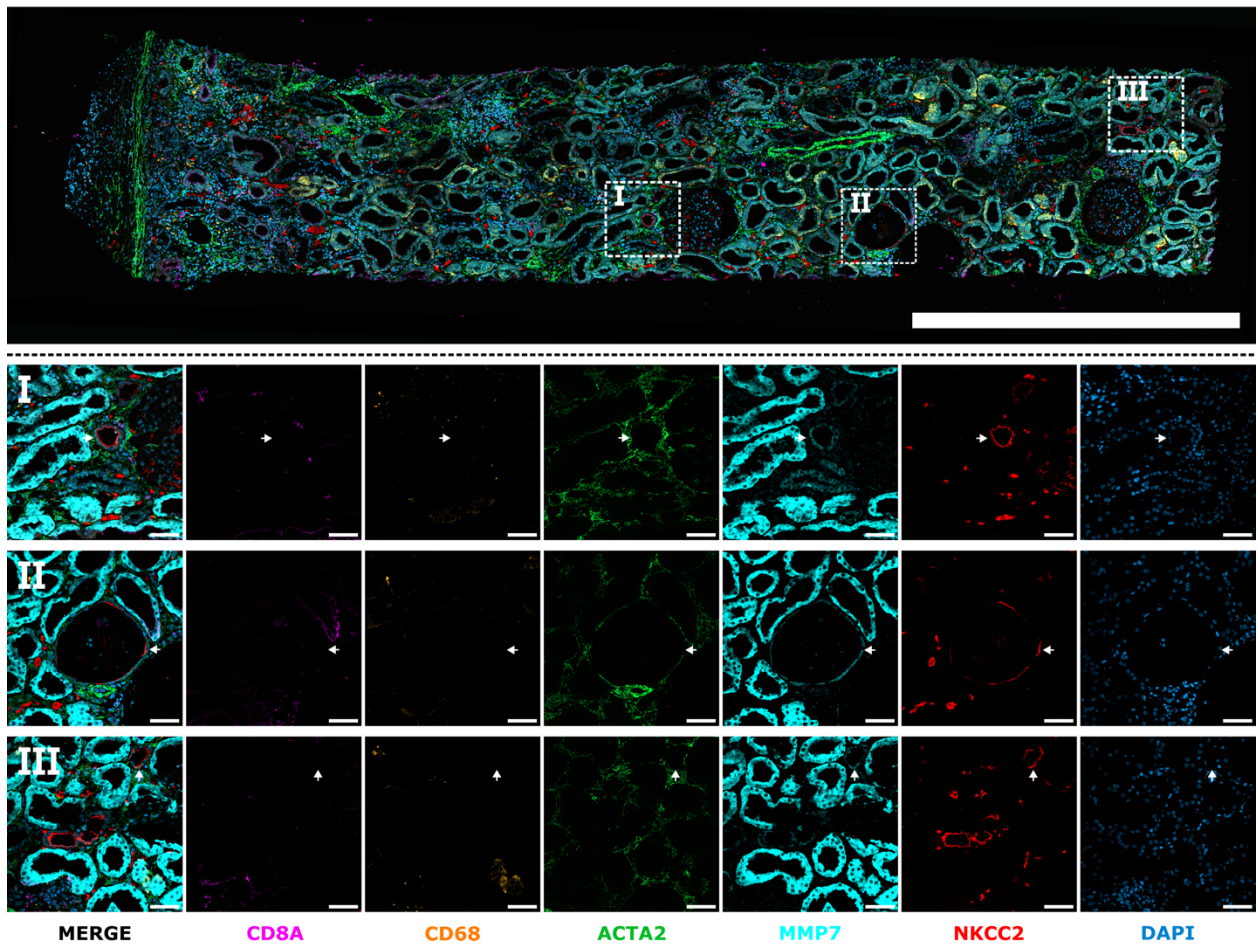
Supplemental Figure S21: Gene expression profiles of TCMR are conserved across single nuclei and bulk transcriptomics data. **A.** Bulk microarray log2 fold-changes in the top 500 increased and decreased genes in TCMR versus no rejection (NR) were similar among protocol and indication biopsies (N TCMR protocol = 22, N TCMR indication = 140). **B.** Pseudobulk log2 fold-changes in the top 500 increased and decreased genes in TCMR versus NR (from bulk transcriptomics) with fold changes from mouse snRNA-seq pseudobulk on all cells (allogeneic versus syngeneic) were highly correlated. **C.** Pseudobulk log2 fold-changes in the top 500 increased and decreased genes in TCMR versus NR (from bulk transcriptomics) with fold changes from human snRNA-seq pseudobulk on all cells (TCMR versus stable allograft) were highly correlated. Green circles denote individual genes that were differentially expressed in the same direction between assays. Red circles denote individual genes that were differentially expressed in the opposite direction between assays. Solid blue line denotes the fitted regression

in log2 fold changes with 95% confidence intervals. ρ denotes the spearman correlation coefficients with respective p-value. Source data are provided as a Source Data file.

Stable Allograft

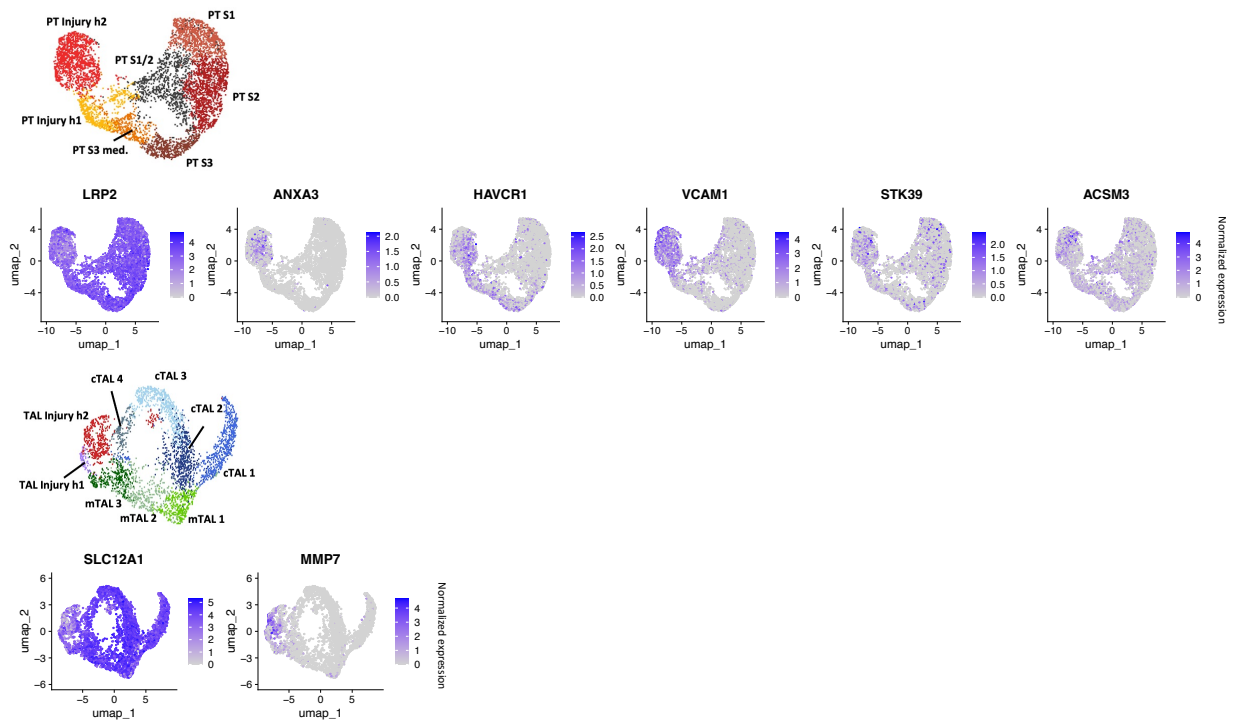


TCMR

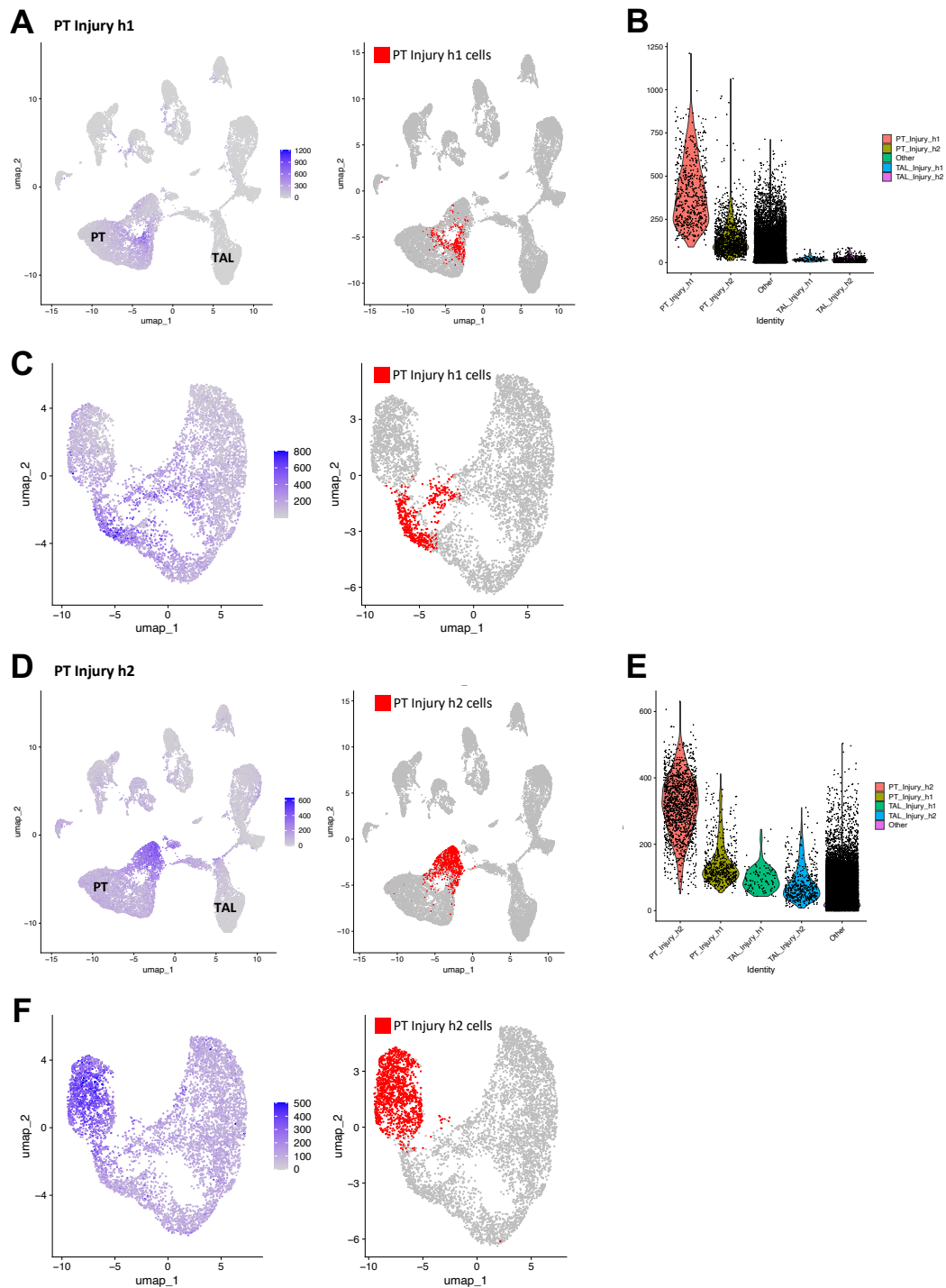


Supplemental Figure S22: Representative overview and inset images of microenvironments surrounding injured TAL cells in kidney biopsy sections from patients with stable allograft function and patients with TCMR. Immunofluorescence staining for T-cells (CD8A, magenta), macrophages (CD68, yellow) and fibroblasts (ACTA2, alpha-smooth

muscle actin, green). Injured TAL cells (TAL Injury h2) (arrowheads) are identified by expression of NKCC2 (red) and MMP7 (cyan). Nuclei are stained with DAPI (blue). Scale bars of overview images: 1000 μ m. Scale bars of insets: 50 μ m. All experiments repeated three times with similar result.

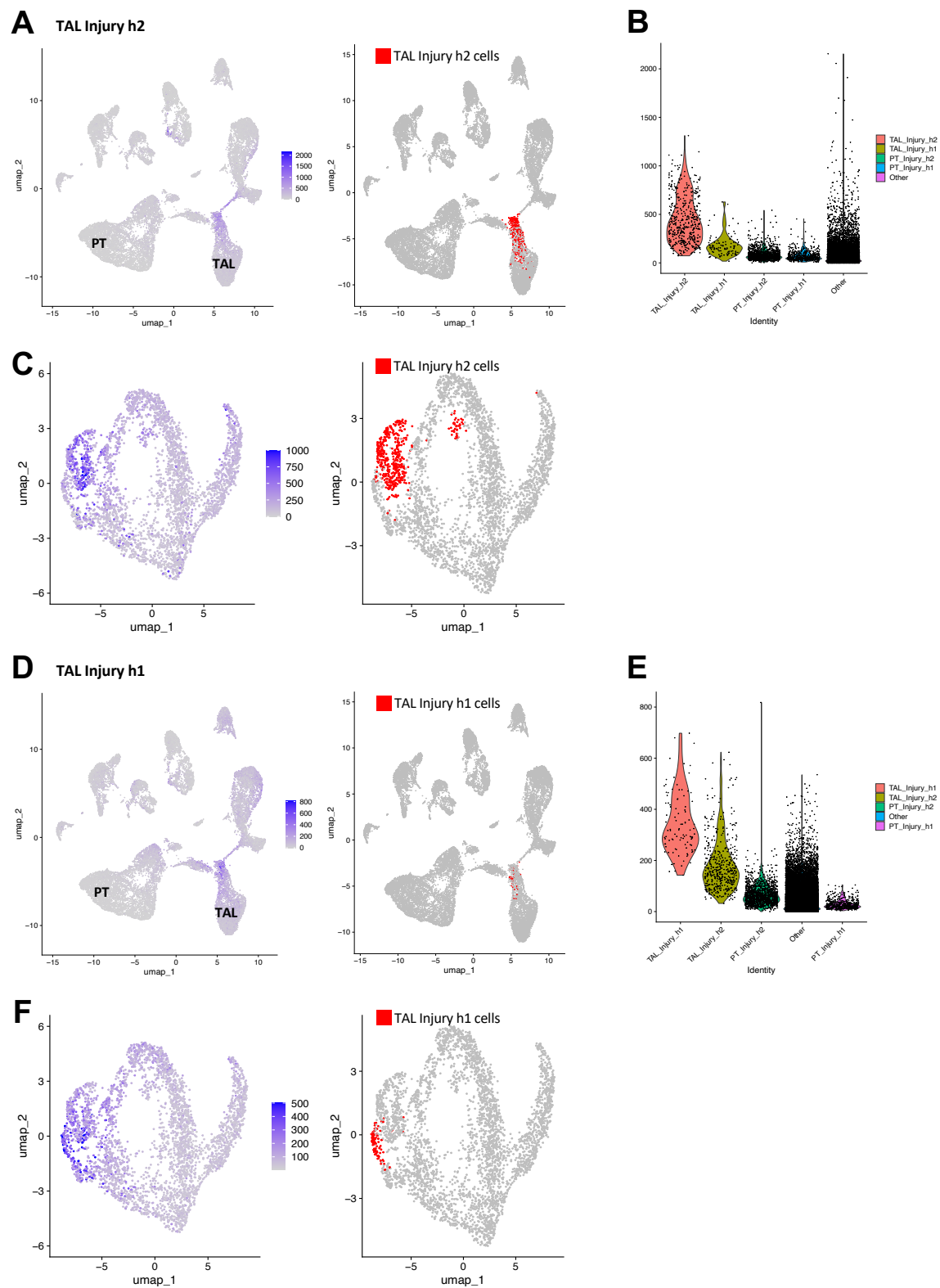


Supplemental Figure S23: Expression domains of selected PT and TAL marker genes. Marker genes include all genes used in immunofluorescence validation for PT Injury h2 and TAL Injury h2 as well as canonical markers LRP2 for PT and SLC12A1 for TAL (Fig. 7, Suppl. Fig. S22).

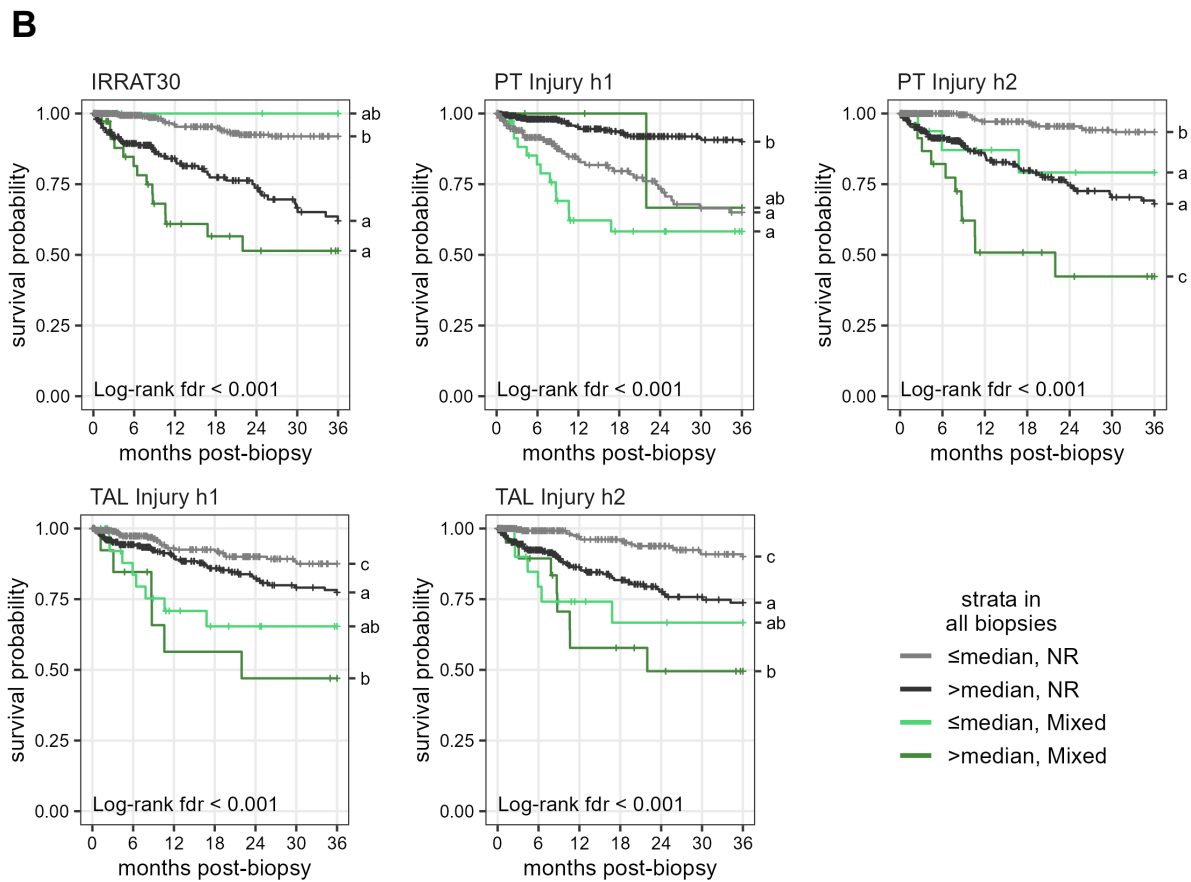
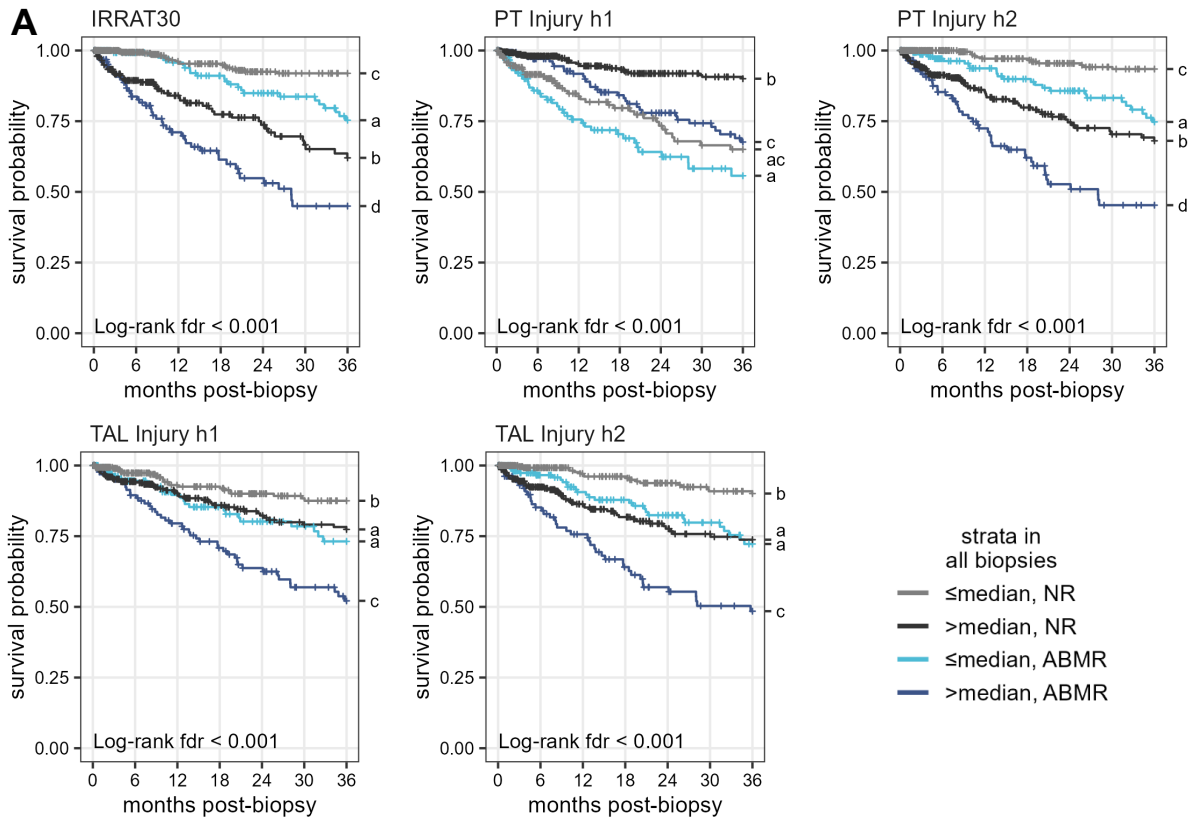


Supplemental Figure S24: Expression patterns for PT gene set scores on human snRNA-seq data. **A.** Feature plot for gene set score for PT Injury h1 on all human cells (average counts per million) (left plot), UMAP highlighting PT Injury h1 cells (right plot) and **B.** violin plot showing average counts per million per cell in all PT and TAL injury clusters and all other cells ("Other").

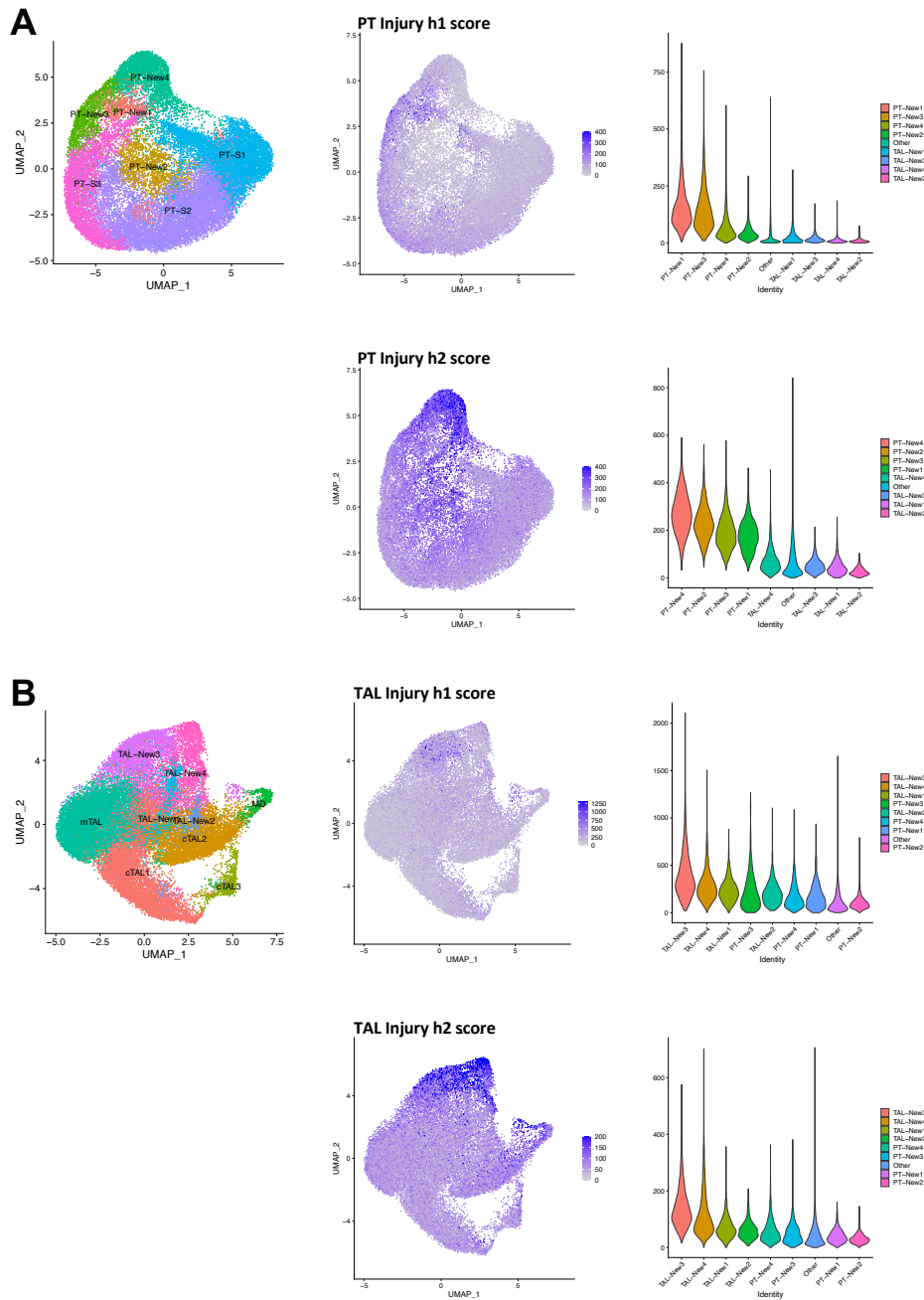
C. Feature plot for gene set score for PT Injury h1 on all human PT cells (left plot) and UMAP highlighting PT Injury h1 cells (right plot). **D.-F.** Analogous plots for PT Injury h2.



Supplemental Figure S25: Expression patterns for TAL gene set scores on human snRNA-seq data. Plots are analogous to Fig. S24 for TAL Injury h1 and h2 cells.



Supplemental Figure S26: Impact of gene set score on patients with ABMR and mixed rejection. A. and B. Kaplan Meier curves for allograft survival in cohort of 1061 kidney transplant biopsies (analogous to Fig. 8 for TCMR). Survival is plotted for ABMR (panels under A.), mixed (panels under B.) (TCMR and ABMR) and NR patients below and above the median score of the respective gene set in the full cohort. False discovery rates (fdr) were derived from log-rank test. Identical letters on the right-hand side of the plot indicate no statistical difference. Source data are provided as a Source Data file.



Supplemental Figure S27: Expression patterns for TCMR-induced PT and TAL injury gene set scores on human AKI data. A. UMAP of PT subclustering as presented in Hinze et al. 2022. This subclustering includes AKI-induced injured PT cell states PT-New 1-4. Feature plots and violin plots are showing the average counts per million score per gene set on the indicated cell populations. **B.** Analogous plots for AKI-induced TAL cell states TAL-New 1-4.